Emerging Challenges in Textile Energy Electrodes: Interfacial Engineering for High-Performance Next-Generation Flexible Energy Storage Devices

Woojae Chang, Euiju Yong, Yoon Jang Chung,* Yongmin Ko,* and Jinhan Cho*

The development of highly conductive fibril-type textile electrodes is crucial for the advancement of various smart wearable electronics including high-performance energy storage devices. To achieve this goal, it is essential to convert insulating textiles into conductive counterparts while maintaining flexibility and porosity. Additionally, the incorporation of electrochemically active components into textile conductors enables tailor-made textile energy electrodes for specific applications. Thus, textile conductors act not only as conductors but also as energy reservoirs for energy-active components, providing a facile electron transfer network. However, textile conductors fabricated by most existing methods face challenges such as low conductivity, blockage, and brittleness. One approach to overcome these problems is to utilize interfacial interactions between individual components and textiles. Conductive nanoparticle assembly and electrodeposition based on such rational design result in highly conductive, flexible, and large surface area textile conductors. The subsequent guided assembly of active components creates high-performance textile energy electrodes. This perspective describes how interfacial interaction-based assembly can enhance the performance of textile conductors and textile energy electrodes. It also explores various conductor preparation approaches and recent advances in the field for applications in supercapacitors and lithium-ion batteries.

1. Introduction

Considerable research efforts have been devoted to the development of high-performance electrical conductors and electrochemical energy electrodes that possess metal-like conductivity along with significant mechanical flexibility and a large active surface area. This surge in interest is primarily driven by the rapid proliferation of wearable, portable, and smart electronics that aim to enhance the convenience and quality of our daily lives. Among the myriad of soft and flexible electrode options available, textile conductors and electrochemically active textile electrodes (shortly referred to as "textile energy electrodes") stand out as particularly promising candidates. This is mainly attributed to their remarkable properties, including expansive surface area, mechanical flexibility, and the inherent lightness of textiles composed of numerous fibrils and/or fibers. In particular, the highly entangled three-dimensional (3D) porous structure of the textile, which enables a significantly high specific surface area-to-volume ratio, can offer an important alternative for power supply components that require higher energy density in limited areas and/or volumes. For instance, in energy storage electrodes such as supercapacitors (SCs) and/or batteries, a major challenge is to balance the mass loading of active materials to achieve high energy density while maintaining power density or energy efficiency. A practical and intuitive solution to overcome this dilemma is the development of high-performance textile energy electrodes using highly conductive, flexible, and porous textiles. In particular, the use of these advanced textile electrodes, characterized by their high energy density and mechanical flexibility,

W. Chang, E. Yong, Y. J. Chung, J. Cho
Department of Chemical and Biological Engineering
Korea University
145 Anam-ro, Seongbuk-gu, Seoul 02841, Republic of Korea
E-mail: yoonjang@korea.ac.kr; jinhan71@korea.ac.kr

Y. Ko
Division of Energy Technology
Materials Research Institute
Daegu Gyeongbuk Institute of Science and Technology (DGIST)
333 Techno Jungang-daero, Hyeongpung-myeon, Dalseong-gun, Daegu 42988, Republic of Korea
E-mail: yongmin.ko@dgist.ac.kr

J. Cho
KU-KIST Graduate School of Converging Science and Technology
Korea University
145 Anam-ro, Seongbuk-gu, Seoul 02841, Republic of Korea

J. Cho
Soft Hybrid Materials Research Center
Advanced Materials Research Division
Korea Institute of Science and Technology (KIST)
5 Hwarang-ro 14-gil, Seongbuk-gu, Seoul 02792, Republic of Korea

has the potential to reduce cell size. Moreover, they can be effectively integrated into pouch cell or multistacked cell designs. These advancements have the potential to reduce unit production costs and position these technologies to secure a significant share of the market.[1]

The primary focus of interest in these textile electrodes, which include both textile conductors (i.e., textile current collectors) and textile energy electrodes, is to achieve uniform and robust deposition of electrically conductive and/or energy storage components (i.e., active components) throughout the entire structure, ranging from the exterior to the interior of the insulating pristine textile. Therefore, the successful development of textile electrodes (i.e., textile conductors and textile energy electrodes) must effectively unravel the diverse and complex correlations between all electrode constituents (i.e., pristine textile, conductive components, and active components). These complexities include accounting for the mechanical properties and porosity of the pristine textile, determining the type and thickness (or a degree of surface coverage) of the conductive components, and establishing appropriate interfacial interactions between each and every ingredient of the electrode. In particular, the interfacial interactions between the electrode components play an important role in determining the electrical, electrochemical, and mechanical reliability under repeated operations that entail various structural deformations (i.e., mechanical bending, pressing, compressing, or twisting).[2] For example, various interfacial interactions such as electrostatic interaction between cationic and anionic components, hydrogen-bonding interaction between amine (NH_2) and carboxylic acid (COOH) (or hydroxyl (OH)) groups, and covalent-bonding interactions between metal (or metal oxide) and NH_2 (or thiol (SH)) groups can be used for robustly incorporating desired components into electrodes, bridging between neighboring active components, and/or depositing the active components onto current collector.

Furthermore, such interfacial design can have a substantial impact on the chemical properties of all exposed surfaces of the textile electrodes, which are deeply involved in their charge transfer kinetics.[3–5] In light of these considerations, the development of textile electrodes for next-generation advanced energy storage devices is highly dependent on the coating qualities of conductive and electrochemically active components based on complementary interfacial interactions.

In order for a textile with the abovementioned physical advantages (i.e., mechanical flexibility and large surface area) to be efficiently utilized as an energy electrode, it is preferentially required to have an electrical conductivity comparable to that of commercial metal conductors such as Ni, Cu, or Al. In this case, it is desirable that all processes to impart electrical conductivity are carried out by solution process under nondestructive, mild conditions to preserve the inherent physical properties of the textiles. Basically, the electrical properties of the textile conductors are directly influenced by the following factors: 1) the type of conductive components incorporated, 2) the coating uniformity of conductive components among the entire region of textile substrates, and 3) their surface coverage onto the textile fibers (i.e., packing density). In most cases, conductive components, such as multiwalled carbon nanotubes (MWCNTs), graphene, metal nanowires (NWs), metal nanoparticles (NPs), and/or conducting polymers, have been incorporated into textiles using

various methods, including physical deposition of conductive suspensions, thermal carbonization, and chemical reduction of metal ions, for the preparation of textile conductors.[6–15] The use of soft conductive components with versatile dimensionality, such as carbonaceous materials and conducting polymers, can be advantageous in terms of mechanical flexibility and expendable active surface area.[6–11] However, their practically lower electrical conductivity (for MWCNTs with an electrical conductivity of ≈ 5.15 S cm^{-1}) or instability (for conducting polymers) in air than that of air-stable metal NPs such as Ag NPs (6.3×10^5 S cm^{-1}) or Au NPs (4.1×10^5 S cm^{-1}) is one of the challenges for their efficient application in energy electrodes.[16–18] Additionally, the above-mentioned strategies (i.e., slurry casting, thermal carbonization, and chemical reduction of metal ions) have generally paid little attention to the interfacial interactions between the textile and the introduced conductive layer, which limits the efficient control of the structural coating quality as well as the mechanical stability of the conductive layer. Therefore, these issues can result in relatively high sheet resistance (1–10^3 Ω sq^{-1}) compared to that of the bulk metal (<0.1 Ω sq^{-1}),[6–8,10,14] clogging of the porous structure by metal agglomerates, and/or poor mechanical flexibility, which can be exacerbated by the additional deposition of energy storage components that typically have poor electrical conductivity.

In terms of the electrical conductivity, one of the most effective ways is to directly introduce densely packed metal NPs instead of carbonaceous materials with intrinsically low electrical conductivity onto the numerous fibrils comprising the textile. At the same time, all interfacial interactions between neighboring metal NPs as well as between metal NPs and textile must also be considered to ensure the coating uniformity throughout the entire area. Furthermore, considering that numerous insulating ligands and/or additives (polymeric linkers) between neighboring metal NPs operate as contact resistances, their mutual separation distance should be minimized to increase the packing density of metal NPs. As an example, Kim et al. reported that thousands of metal NP multilayers consisting of a stacked free-standing film could be prepared by electrostatic layer-by-layer (LbL) assembly based on complementary interaction between anionic Au NPs and cationic insulating polyelectrolytes.[19] Additionally, several free-standing stacked films, consisting of a few hundred NP layers, were thermally pressed to create a well-connected network of Au NPs with reduced separation distance between neighboring NPs. As a result, these films exhibited high electrical conductivity, reaching approximately 10^4 S cm^{-1}. However, it should be noted that interfacial assembly, relying on electrostatic interactions between cationic and anionic components in aqueous media, faces challenges when attempting to increase the loading amounts of active components, especially metal or metal oxide NPs. This difficulty arises from the long-range electrostatic repulsion between the same charged components. On the other hand, LbL assemblies, which can also take place through hydrogen-bonding or covalent-bonding interactions in organic media, can effectively increase the packing density of adsorbed conductive components. Despite environmental friendliness and easy of application of conventional LbL assembly methods on substrates with various and complex dimensions, still the presence of organic ligands

**ADVANCED
SCIENCE NEWS**

www.advancedsciencenews.com

**small
structures**

www.small-structures.com

existing at the interfaces of conductive components still significantly increases contact resistance. Moreover, achieving the desired packing density of conductive components on host substrates requires multiple deposition processes.

Recently, it has been reported that a ligand replacement reaction-based LbL (LRR–LbL) assembly using ligand exchange between bulky organic ligands bound to the surface of the metal NPs and small molecular linkers can generate the highly flexible textile conductors with high electrical conductivity ($\approx 10^5$ S cm^{-1}), while maintaining a large surface area of pristine textile.[20–22] This approach using a small molecular linker-induced ligand replacement significantly reduced the separation distance between adjacent spherical-type metal NPs, which could consequently induce the high electrical conductivity comparable to that of the bulk metals. However, as the LRR–LbL assembly still requires tens of metal NP multilayers, such a time-consuming process restricts its commercial applications. Therefore, more efficient approaches for the preparation of highly conductive textiles and the resulting textile energy electrodes have been strongly demanded. As an alternative, a recently introduced combinatorial approach involving LRR–LbL assembly and metal electroplating process has shown great promise in significantly reducing the preparation time for textile conductors with bulk metal-like electrical conductivity. This is achieved by performing metal electroplating on the textile with a few metal NP layers (i.e., the textile with minimal electrical conductivity suitable for metal electroplating).[23–29]

To utilize textile conductors as the basis for textile energy electrodes including SCs or various types of batteries (e.g., lithium-ion batteries (LIBs), lithium-sulfur (Li–S), or lithium-air (Li–O$_2$) batteries), active components, such as transition metal oxides (TMOs), are further incorporated by the conventional slurry casting process.[15,30–32] However, the presence of insulating polymer binders in the slurries poses a challenge to efficient charge transfer between adjacent active components, resulting in numerous contact resistances at their interfaces. To overcome this limitation, a similar approach to that used for the aforementioned textile conductor can be used to form textile energy electrodes. That is, by using an additional LRR–LbL assembly technique, the active components can be robustly deposited onto the textile conductors, resulting in high-performance textile energy electrodes.

In this perspective, we are thoroughly investigating various textile conductors and textile-based energy storage systems, such as SCs and LIBs. Our investigation focuses on the critical role of interfaces between electrode components and the conformal and dense assembly of conductive components, and active components on textile fibrils in determining the overall performance of energy storage electrodes.

We begin by reviewing the fabrication of textile conductors, which involves the use of various conductive components and their corresponding deposition processes (**Scheme 1**). We consider the structure and mechanical properties of the conductive layer (film) formed on the textile surface by each approach and examine their impact on the electrical properties of the resulting textile conductors. In particular, we present the successful application of the LRR–LbL assembly of conductive components, which has led to the production of textile conductors with exceptional electrical conductivity. These textile conductors hold immense potential to serve as efficient energy reservoirs and
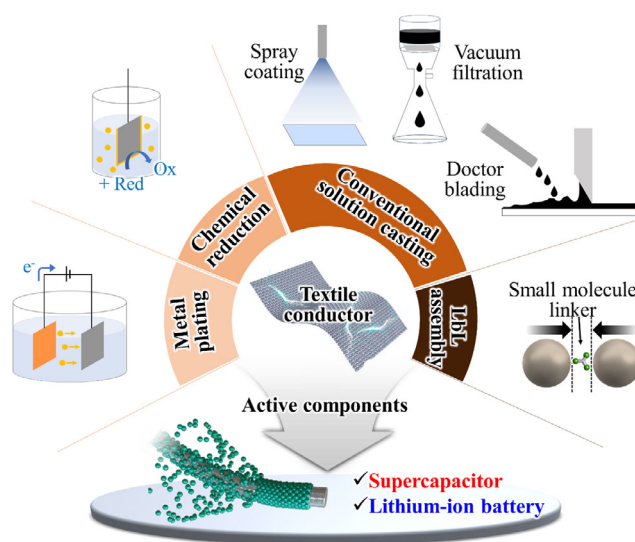
Scheme 1. Schematic illustration of various approaches for the fabrication of textile conductors applicable as current collectors for energy storage systems, such as supercapacitors and lithium-ion batteries.

act as current collectors for a wide range of energy storage electrodes. Here, we shift our focus to textile current collector-based SCs and LIBs, emphasizing the importance of interfacial interactions in enhancing the overall energy performance of textile energy electrodes, as well as the charge transfer kinetics between adjacent active components within the electrodes. We review a variety of reported approaches that have shown promise in this regard. Finally, we briefly outline key areas for improvement in textile electrodes to pave the way for future advances in energy storage devices. We hope that this perspective will prove invaluable to the energy storage community and accelerate the research and development of superior textile electrodes specifically tailored for wearable and smart electronics applications.

2. Preparation of Textile-Based Electrical Conductors

In general, natural textiles such as cotton, silk, and paper have intricate porous fibril structures that are characterized by a significantly large specific surface area, mechanical flexibility, light weight, and suitability for seamless integration into various flexible electronic applications.[32–36] However, the exceptional properties of these natural textiles also present notable challenges in achieving a high-quality conductive layer necessary to achieve the desired level of electrical conductivity. In particular, to fully exploit the physical advantages of natural textiles in flexible conductors, it becomes crucial to ensure sufficient surface coverage, uniformity, density, and appropriate film thickness of the conductive layer over all exposed areas of the textiles. Careful attention must also be given to avoid blockages in the voids within the porous textile resulting from the agglomeration of conductive components. Effective control of these coating conditions can be more efficiently achieved by well-defined favorable interactions between the electrode components, as discussed in the

Section 1. This critical aspect facilitates the optimal exploitation of the properties of the textile.

The following section provides a comprehensive overview of various approaches (casting, dipping, spraying, printing, electroless deposition, sputtering, electroplating, LbL assembly, etc.) to the preparation of textile conductors, with particular emphasis on interfacial (or surface) design. The importance of this design is emphasized to ensure the mechanical, structural, and electrical reliability of the textile electrode, thereby enabling its successful incorporation in textile-based energy storage applications.

2.1. Conductive Suspension-Based Coating

The presence of numerous hydrophilic groups, such as glucose molecules (including hydroxyl groups) and amino acids, in traditional textiles plays an important role in promoting excellent surface wettability. This property is beneficial in enhancing the processability of solution-based deposition techniques. As a result, a wide range of conductive liquid–solid suspensions, including slurries and inks containing conductive components, such as conductive polymer or carbon compounds, can be applied directly to textiles through conventional processes (i.e., casting, dipping, spraying, or printing).[6,8,9,37–48] For example, Dudem et al. fabricated electrically conductive textiles by a simple dipping process of common wearable clothes (i.e., worn-out cotton textiles, WCTs) into an aqueous solution consisting of a mixture of aniline hydrochloride and ammonium peroxydisulfate, thereby inducing an in situ polymerization or growth of polyaniline (PANI) on the WCTs (PANI@WCTs) (**Figure 1**a).[38] In such deposition processes, the electrical conductivity of the resulting textile conductors, specifically the conductive layer deposited onto the textile surface, primarily depends on the concentration of the conductive fillers in the suspension, which is closely related to the electron percolation behavior.[8,45,49] As a result, the electrical conductivity of the formed PANI@WCTs exhibited a gradual increase with increasing deposition time (or loading amount) of PANI, with the lowest sheet resistance of $7800\,\Omega\,sq^{-1}$ at a deposition time of 30 h (Figure 1b). In a similar way, Xu et al. developed textile-based current collector for Li–O$_2$ battery cathode through a dip-coating process, wherein the textile fabric was repeatedly dipped into a $10\,mg\,mL^{-1}$ single-walled carbon nanotube (SWCNT) ink.[47] This approach yielded bendable and twistable textiles with exceptional mechanical strength. The single fiber of SWCNT-coated textile exhibited a resistance of $1250\,\Omega$ and a conductivity of $50\,S\,cm^{-1}$, while the entire textile exhibited resistances of approximately $227\,\Omega$ and conductivities of $125\,S\,cm^{-1}$, respectively. These results showed the effectiveness of dip-coated SWCNT networks, providing facile electron transport pathways.

In addition, it is essential to achieve optimum coating quality for the conductive layer is paramount, as it directly affects both the electrical conductivity and physical properties of the textiles. This quality is highly dependent on various fluid properties of the suspension, including viscosity, density, surface tension, homogeneity of the components, and dispersion stability of the conductive fillers.[50–53] Furthermore, this critical property of the conductive suspension is influenced by a complex interplay of the content and composition of its components, such as the conductive filler, solvent, and functional additives (e.g., binder, surfactant, and rheology modifier). The intricate combination of these elements plays a significant role in determining the behavior of the fluid during the deposition process.

Paradoxically, however, such functional additives, which are essential for achieving the desired levels of mechanical robustness, structural integrity, and electrical conductivity of the textile conductors under various mechanical deformations, can pose a challenge by impeding facile electron communication at the interfaces of each conductive component within the electrode due to their insulating nature. Although various types of carbon materials, such as carbon nanotubes (CNTs) or graphene nanosheets, have been continuously used in additive (i.e., binder and surfactant)-free coating approaches based on the surface functionalization or their self-bundling nature, their relatively low electrical properties compared to bulk metals often limit the suitability for applications in energy storage systems requiring high energy and power efficiency.[54–58] On the other hand, metal nanomaterials (i.e., metal NPs or NWs) generally require a sufficient amount of polymeric binders or ligands to form a stably and uniformly cross-linked three-dimensional (3D) network that can effectively confine the metal components. Therefore, these coating processes typically require additional posttreatments such as chemical or electrical sintering, thermal annealing, laser irradiation, and flash light welding to eliminate the insulating polymeric species and form a well-connected conductive (metallic) network.[59–66] For example, a flash light (e.g., xenon lamp) sintering process with an irradiation time of a few microseconds has been employed to create a well-connected metallic layer on the flexible soft substrates, such as plastics or fabrics (Figure 1c).[67] For this, metal nanomaterial (i.e., NP or NW)-based layers are preferentially deposited onto the substrates through dipping or printing of conductive suspensions. In this case, the electrical conductivity and mechanical properties of the resulting flexible conductors are strongly influenced by various parameters, including the coating (deposition) quality of the metal layer, the loading amount of metallic species, and the energy density and pulse duration of the light irradiation. That is, the higher amounts of metallic fillers are expected to result in better electrical conductivity. However, achieving the higher electrical conductivity often requires higher irradiance, which in turn can lead to poorer mechanical properties and significant physical damage to the textile substrates, as confirmed by field-emission scanning electron microscopy (FE-SEM) images (Figure 1d). Thus, it is worth noting that such posttreatment processes can involve relatively harsh process conditions, such as high annealing temperature or focused high-energy photonic welding, which unfortunately limit the range of textiles that can be effectively used in these applications.

To address this issue, researchers have explored the use of additive-free conductive inks for inkjet or extrusion printing to fabricate flexible or wearable electronics.[68–71] One example of such an ink is MXene, which has high electrical conductivity (intermediate between carbon materials and metals) and hydrophilic surface functionality with a negative electrostatic charge. These MXenes can be stably dispersed in water or polar organic solvents without any additives, allowing them to be directly printed onto flexible substrates as a current collector and energy electrode.[68,69] Zhang et al. successfully formulated
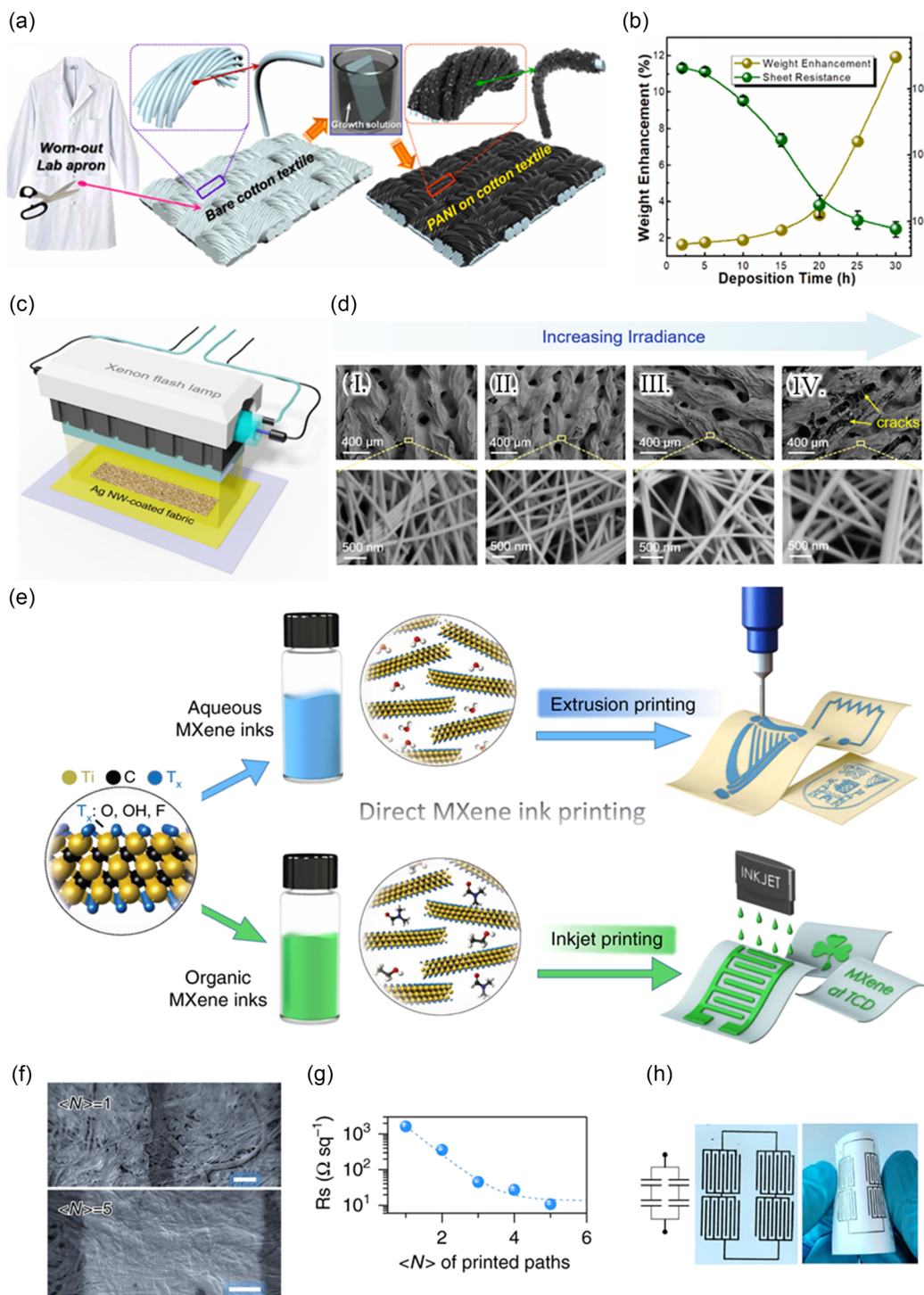
Figure 1. a) Schematic illustration showing the fabrication of PANI@WCT conductors *via* an in situ polymerization of PANI on the WCTs using a dip-coating process. b) Deposition time (h)-dependent weight enhancement (%) and sheet resistance value of PANI@WCTs. Adapted with permission.[38] Copyright 2019, Elsevier. c) Schematic illustration of flash light sintering process for Ag NW-fabrics. d) FE-SEM images of Ag NW-fabrics for irradiance of 0 kW cm^{-2} (I), 6 kW cm^{-2} (II), 10 kW cm^{-2} (III), and 16 kW cm^{-2} (IV), respectively. Adapted under the terms of the CC-BY Creative Commons Attribution 4.0 International License.[67] Copyright 2018, the Authors. Published by Springer Nature. e) Schematic illustration of direct MXene ink printing process on paper substrate and the changes of f) the surface FE-SEM images, and g) the sheet resistance as a function of printed paths. h) Extrusion printed on a paper substrate (left), showing a great flexibility (right). Adapted under the terms of the CC-BY Creative Commons Attribution 4.0 International License.[68] Copyright 2019, the Authors. Published by Springer Nature.

and directly printed additive-free, concentrated MXene inks onto untreated paper substrates for micro-supercapacitors (MSCs) (Figure 1e).[68] By increasing the printed number through extrusion printing, they achieved a remarkable reduction in sheet resistance, resulting in the creation of a well-percolated nanosheet network (Figure 1f,g). Notably, the elimination of the need for a polymeric binder was made possible by the strong hydrogen bonds formed between the multistacked MXene sheets and the substrate. This breakthrough enabled scalable production and enhanced mechanical stability of the printed substrates (Figure 1h). To optimize the rheological properties of these conductive inks, adjustments are made to the filler content (concentration) and the properties of the organic solvent, which, in turn, depend on the type of substrate to be coated.[72] However, the need for a high filler content to ensure high resolution and electrical conductivity can result in poor penetration behavior into highly porous textile substrates, limiting the full utilization of the physical advantages of the textile, such as its large specific surface area that ensure mass loading of active components.

An alternative approach to achieve high electrical conductivity while preserving the physical and mechanical properties of soft textiles is the room temperature sintering of metal NPs.[65,66,73] This phenomenon is driven by the reduction of the diffusion barrier for metal atoms at the interface between adjacent metal NPs, which can be induced through proper surface design of the NPs to minimize the surface chemical potential. For example, the introduction of specific surface-active organic molecules to the as-deposited metal NP-based film leads to the desorption of native polymeric stabilizer (ligand) bound to the NP surface, destabilizing the metal atoms on the surface.[65,66] This process triggers the spontaneous coalescence of adjacent metal NPs through atomic diffusion and surface relaxation on the NP surface to reduce the surface energy,[74,75] resulting in the formation of a stable interconnected metallic network. Importantly, this approach requires a sufficiently short interparticle distance to facilitate atomic diffusion, which can be achieved through a concentrated, homogeneous metal NP-based suspension. Consequently, the room-temperature sintering in a metal NP suspension-based coating process can occur in densely packed NP arrays after solvent evaporation. Given that the spontaneous coalescence of metal fillers under mild conditions (i.e., room temperature) is more favorable at the nanoscale,[76,77] the proper optimization of the metal NP contents and the rheological properties (especially viscosity) is one of the essential challenges to effectively utilize the textile substrates.

2.2. Chemical Deposition for the Preparation of Metallized Textile Conductors

The preparation of metallized textile conductors using a solution-based chemical deposition process provides an efficient and effective means of creating a conductive layer on textiles with hydrophilic groups. This deposition method is carried out under relatively mild conditions, which ensures a comparatively uniform surface coverage of metal components onto textiles, while maintaining mechanical reliability. In this section, we present a range of representative chemical deposition approaches that utilize different driving forces for the successful creation of metallized textile conductors.

2.2.1. Catalytic Self-Reduction of Metal Ions

Spontaneous chemical reduction of metal ions without an external electric current can be achieved by precisely adjusting the content of functional reagents (such as reducing agents, stabilizers, and buffers) in the reacting bath.[78] In this case, the quality of metal plating on the textile substrate largely depends on the adsorption behavior of the active components. To ensure a uniform and strong adsorption of catalytic active sites capable of anchoring and reducing the metal ions, the textile surface should be carefully functionalized (sensitized) using various vapor- or solution-phase deposition methods.[14,15,79–85] One highly efficient solution-based sensitization process is polymer matrix-assisted electroless plating, which allows well-defined and strong interactions between the polymer matrix and the catalysts as well as between the textile substrate and the polymer matrix.[15,86–88] That is, in the case of grafting functional polymers onto the textile surface, they immobilize the ionic catalyst complex by electrostatic attraction and act as reduction sites for metal ions. For example, Lin et al. successfully fabricated a stretchable knitted-textile conductor by polymer-assisted copper (Cu) electroless deposition process (**Figure 2**a).[88] In this study, a polymer matrix (i.e., polydopamine, PDA) was formed by immersing textile in a dopamine solution (pH 8.5) and polymerized at room temperature for 12 h, which provided anchoring sites for the $PdCl_4^{2-}$ catalyst to form the subsequent Cu layer in the electroless deposition process. As a result, the Cu textile exhibited a low sheet resistance of $\approx 0.32\,\Omega\,sq^{-1}$ and exhibited 500% stretchability with a high level of conductivity retention ($\approx 2.0\,\Omega\,sq^{-1}$) (Figure 2b).

During this electroless plating (i.e., chemical reduction) process, the electrical conductivity gradually increases over time due to the progressive formation of a thick and robustly bonded metal layer on the substrate by rapid and continuous reduction of metal ions.[85,86,89] However, this characteristic can also lead to the uneven distribution and aggregation of metal clusters, potentially clogging the pore structures of the textile and significantly limiting its physical properties. In addition, chemical impurities, such as residual catalysts or reducing agents within the formed metal composite layer, may hinder the efficient achievement of higher electrical conductivity, especially in thinner metal layers. Therefore, achieving high-quality textile electrodes requires a precise control of the process parameters.

2.2.2. Metal Electroplating Deposition

Another effective approach to convert insulating textiles into metallized textiles is a metal plating deposition by the chemical reduction of metal ions under an external current.[90] In this case, the uniform contribution of the external current applied to the substrate during metal electroplating is a critical parameter that ensures the formation of a high-quality conducting or functional layer. However, for metal electroplating of nonconductive flexible substrates like natural textiles, a conductive seed layer with adequate electrical conductivity
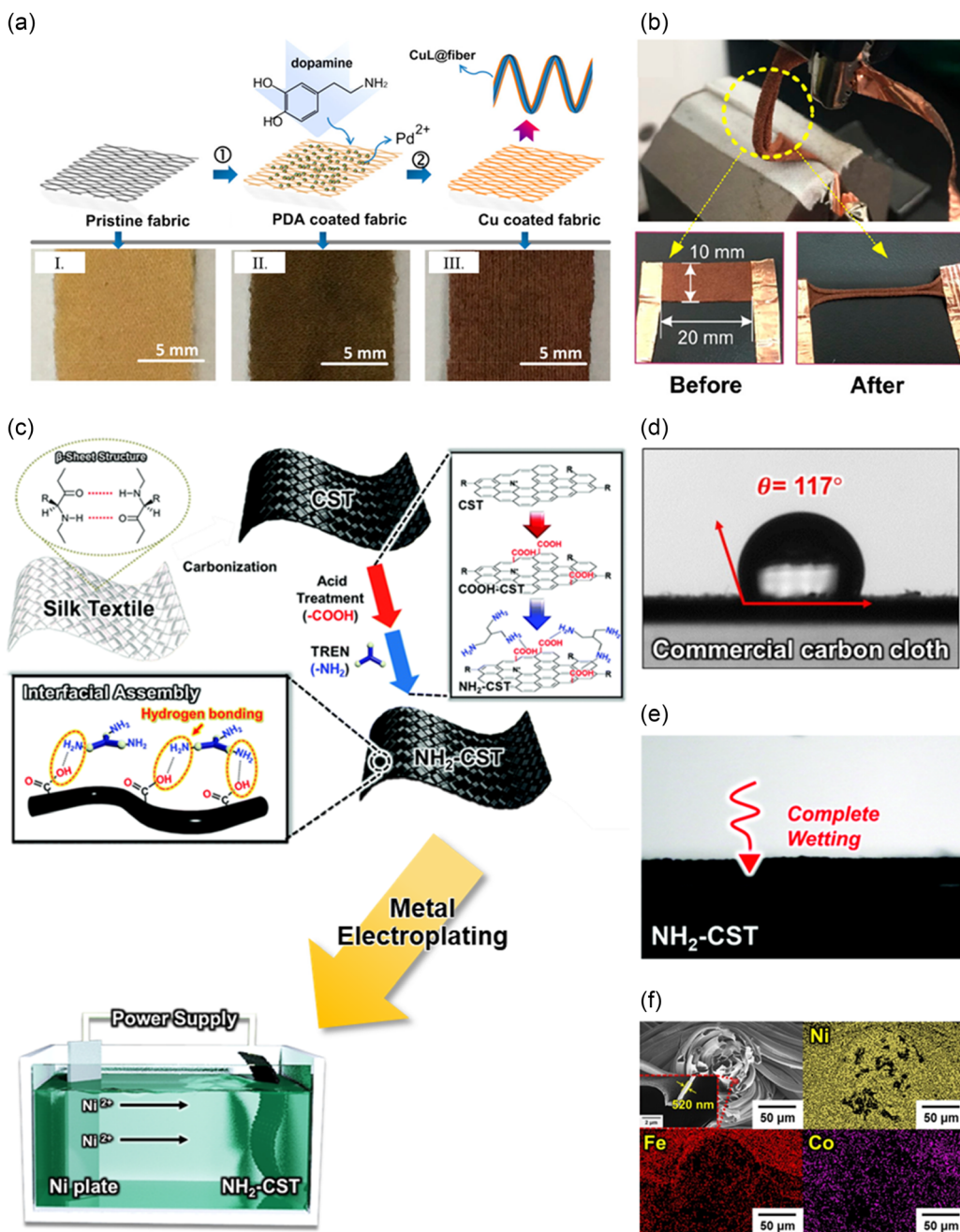
**ADVANCED
SCIENCE NEWS**

www.advancedsciencenews.com

**small
structures**

www.small-structures.com

Figure 2. a) Schematic illustration of polymer (PDA)-assisted electroless deposition process and digital images corresponding to each process step: (I) pristine fabric, (II) PDA-coated fabric, and (III) Cu-coated fabrics. b) Digital images for mechanical stretching test of Cu-coated fabric. Adapted with permission.[88] Copyright 2019, American Chemical Society. c) Schematic diagram of the preparation of conductive silk textiles (CSTs) through carbonization/interfacial assembly-induced metal electroplating method. Water contact angle of d) commercial carbon cloth and e) NH₂-CST. f) FE-SEM and the corresponding energy-dispersive X-ray spectroscopy (EDX) mapping images of electroplated NiFeCo-CSTs. Adapted with permission.[97] Copyright 2022, the Authors. Published by The Royal Society of Chemistry.

should be preferentially coated onto insulating textiles by various physical and chemical deposition methods such as autocatalytic deposition and sputtering.[91–94] Additionally, the precise control of the externally applied electric field can induce the formation of highly uniform metallized layer onto the textile surface.

Metal electroplating on the conductive seed layer-coated textile (i.e., conductive textile) induces atom-to-atom interdiffusion into lattice vacancies, a process known as interfacial site exchange. This phenomenon results in strong interfacial adhesion between conductive seed layer and electroplated metal layer, and furthermore generates a robust metallic structure.[95] However, the

interfacial interaction between textile surface and conductive seed layer is essential for ensuring reliable mechanical and electrical performance of the resulting metallized textile conductors. Unfortunately, studies on this aspect have been considerably limited.

An alternative approach for enhancing interfacial adhesion is the carbonization of textile materials. Through a high-temperature carbonization process in an inert environment, the formation of a conjugated system from sp^2 hybridized carbon structure provides an electron transfer pathway, which converts an insulating textile into a conductive textile while retaining some degree of mechanical flexibility without additional chemical and physical treatments.[96–100] For example, Shin et al. reported on the utilization of a Li–S copolymer cathode, which employed a Ni-electroplated textile-based current collector. This collector was prepared through the process of electroplating Ni onto carbonized cotton textile (i.e., EP-CT).[98] The resulting EP-CT demonstrated an exceptionally low sheet resistance of ≈0.01 Ω sq^{-1}, while maintaining a highly porous structure and a large surface area without any metal agglomeration at its surface. Moreover, these EP-CTs proved to be effective current collectors and reservoirs for accommodating high loadings of sulfur copolymers, owing to their extensive surface area and the favorable interfacial interaction between the electroplated Ni layer and the sulfur copolymers. In a related advancement, recent research conducted by Mo et al. has successfully transformed protein-based silk textiles into electrically conductive textiles, known as conductive silk textile. This transformation was achieved through the process of carbonization combined with interfacial assembly-induced metal electroplating (Figure 2c).[97] In this study, the surface of the carbonized CSTs can be further modified with hydrophilic functional organics (i.e., amine (NH$_2$)-functionalized small organic molecules; tris(2-aminoethyl)amine, TREN) through subsequent acid treatment. As confirmed by the water contact angle test, this surface modification using the hydrophilic organics (TREN) enables the complete wetting of water, in contrast to the commercial carbon cloth without surface modification (Figure 2d,e). This phenomenon can induce the favorable interfacial interaction between the hydrophilic functional organics of carbonized textile and the electroplated metal layer, ensuring uniform and stable metal layer on the CST surface. Furthermore, this approach can also allow efficient and uniform incorporation of various electrochemically active metal/metal oxide materials (e.g., NiFeCo) through additional electroplating for flexible energy electrode applications (Figure 2f). However, the conversion of organic composition and chemical structures of natural fibers into comparatively brittle carbon-rich structures of carbonized fibers must accept some loss of mechanical flexibility of the textile.

Another promising approach is the deposition of metal NP-based thin films using an LRR–LbL assembly technique. Metal NPs dispersed in a nonpolar solvent can be covalently bonded to NH$_2$-functionalized small organic molecules due to the high affinity between the surface of metal NPs and the amine groups of organics, forming a densely and uniformly packed metal NP-based thin layer on the textile surface. This arrangement allows efficient electron transfer between neighboring metal NPs, leading to high electrical conductivity suitable for efficient electroplating. Moreover, the electrical conductivity of the LbL-assembled metal NP film can be further improved by adjusting the number of deposition layers, enabling the achievement of bulk metal-level electrical properties without the need for additional metallization processes. The details of this approach are discussed in the following section.

2.3. Self-Assembly of Metal Nanoparticles

The direct deposition of the as-synthesized, high-quality (e.g., controlled size and narrow size distribution) metal NPs onto the textile can be more suitable than employing the spontaneous metal ion reduction processes. Additionally, self-assembly of the metal NPs, based on the well-defined, strong interactions between each NP and the substrate, is more favorable to form a thin film with highly uniform structure, which can minimize the loss of mechanical and physical properties of the textiles.

The organic ligands (i.e., stabilizer) attached to the NP surface not only provide size uniformity and dispersion stability in the desired solvents but also serve as binding sites (mainly through hydrophilic moieties) for the complementary interaction with other functional materials.[101] However, the insulating property of organic ligands, especially those with long and/or bulky chains that provide higher dispersion stability in nonpolar solvents,[102] can significantly impede electron transfer at the interfaces, both between adjacent NPs and between NPs and the substrate. Recently, our group and coworkers reported a ligand engineering (i.e., replacement)-mediated LbL assemblies of metal NPs for the preparation of textile conductors with high electrical and mechanical performance under mild conditions. In this section, we discuss the recent progress and impacts of the LbL assembly approach, which involves the proper surface (or interface) design, for the preparation of highly conductive textile electrodes.

2.3.1. Ligand Replacement Reaction (LRR)-based Layer-By-Layer (LbL) Assembly

The LbL assembly method is a versatile solution process that allows the preparation of thin film-type nanocomposites with tailored functionalities based on well-defined complementary interactions between the material components on various types of substrates.[103] Traditional LbL assemblies are mainly carried out based on the electrostatic attraction of oppositely charged components in aqueous media and/or the hydrogen-bonding interaction in aqueous or alcohol media, which allow precise control of the physical and chemical properties through the adjustment of various experimental parameters (**Figure 3**a,b).[19,104–109] However, the conventional LbL assemblies of metal NPs with charged capping ligands (i.e., stabilizers) have difficulty in achieving the densely packed NP arrays (i.e., large interparticle distance) due to the long-range electrostatic repulsion between same charged NPs. Furthermore, large amounts of organic ligands remaining at NP–NP interfaces within the formed composite films significantly increase contact resistance and electron scattering, leading to a higher electrical percolation threshold.

Alternatively, it has been reported that hydrophobic metal (or metal oxide) NPs can be directly LbL assembled with hydrophilic small-molecule linkers *via* covalent bonding interactions in organic media.[110–114] In this process, the hydrophobic organic
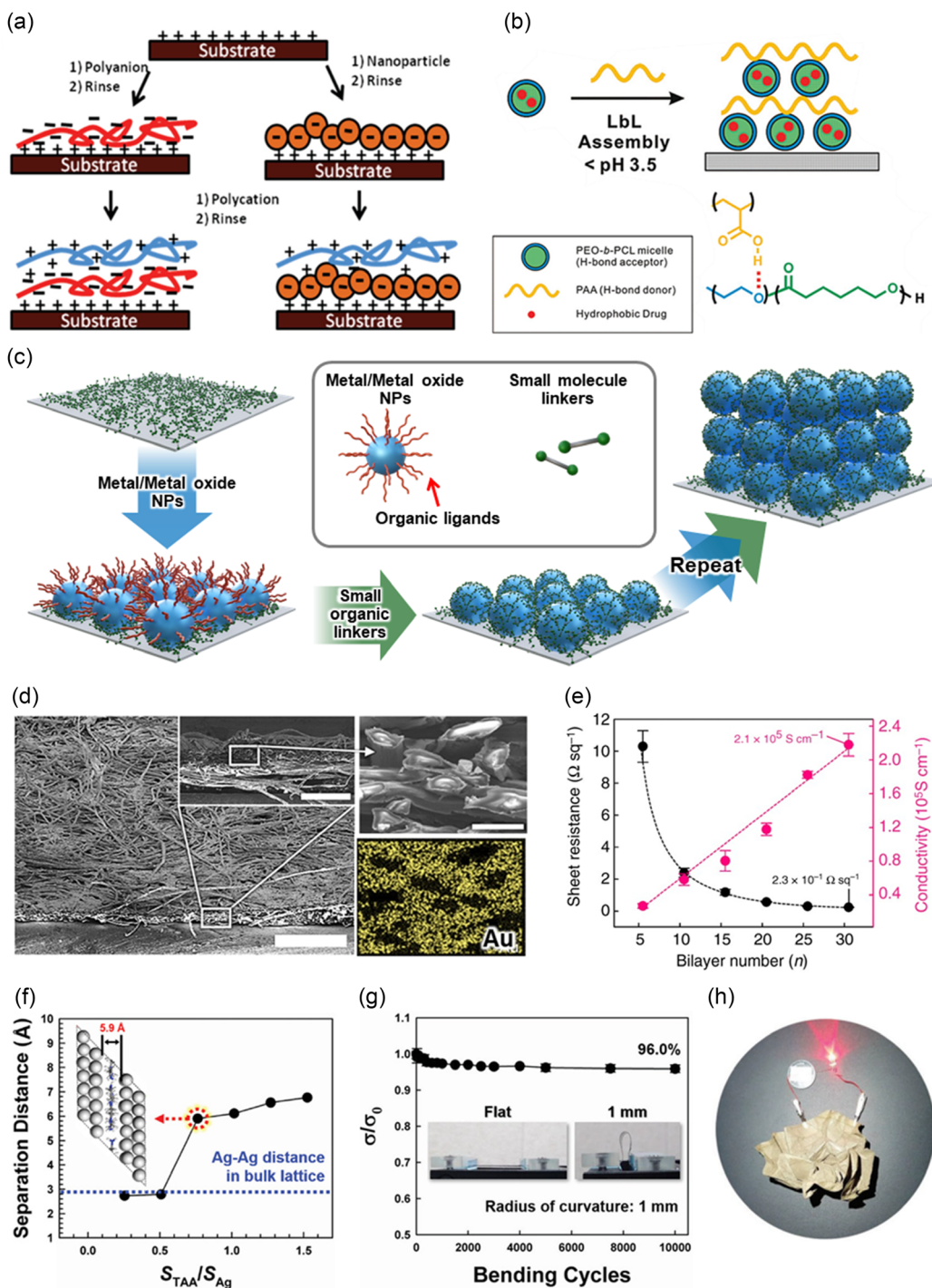
Figure 3. Schematic illustration of traditional LbL film deposition process based on a) electrostatic attraction and b) hydrogen-bonding interaction. a) Adapted with permission.[106] Copyright 2008, American Chemical Society. b) Adapted with permission.[109] Copyright 2008, American Chemical Society. c) Schematic illustration of LRR–LbL assembly. d) FE-SEM and EDX images of (TOABr-Au NP/TREN)$_{10}$-coated textile (scale bars indicate 500 μm (left), 200 μm (inset), and 20 μm (right), respectively). e) Sheet resistance and electrical conductivity property of (TREN/TOABr-Au NP)$_n$-coated textiles as a function of the bilayer number (n). d,e) Adapted under the terms of the CC-BY Creative Commons Attribution 4.0 International license.[20] Copyright 2017, the Authors. Published by Springer Nature. f) Atomistic molecular dynamic (MD) simulation results showing the minimum separation distance between adjacent Ag atoms separated by TAA molecules in bulk Ag lattice as a function of surface coverage ratio (S_{TAA}/S_{Ag}). g) Bending cycle number-dependent electrical property (σ/σ_0, where σ_0 indicates the electrical conductivity of the initial state) of Ag NP-coated textile conductors. h) Photographs of crumpled Ag NP-coated textile conductor connected to a red LED. Adapted with permission.[22] Copyright 2019, Wiley-VCH.

ligands loosely bond to the NP surface are effectively removed and replaced by the incoming organic linkers during LbL assembly (Figure 3c). This LRR takes place because organic likers have a stronger binding affinity to the NP surface, which is attributed to the presence of high-affinity functional groups (e.g., halides and amines) and/or chelate effects.[115–117] This LRR–LbL assembly is characterized by the fact that the interparticle distance within the LbL-assembled metal NP-based films can be significantly reduced by modulating the molecular weight (related to the chain length or size) of the organic linkers, thereby enabling both high NP-packing density and the reduction of contact resistance. Based on this approach, Ko et al. reported a metallic textile conductor *via* a small molecule linker (TREN)-mediated LRR–LbL assembly of hydrophobic Au NPs (stabilized by tetraoctylammonium bromide, TOABr) and applied it as a current collector for flexible all-solid-state SCs.[20] Specifically, the hydroxyl group (OH)-functionalized cellulose paper textile was first immersed in TREN solution (in ethanol) for an adequate adsorption period. Subsequently, it was thoroughly rinsed with pure ethanol and air-dried, respectively. Following these steps of immersing, rinsing, and drying, the outermost layer of textile was effectively coated with NH_2-functionalized TREN linker through hydrogen bonding interactions. The resulting TREN-coated textile was then immersed once more time in TOABr-Au NP solution (in toluene). Afterward, it underwent a similar process of thorough rinsing with pure toluene and air-drying. In this case, the NH_2 groups within the TREN linker establish a robust coordination bond with the Au NP surface, leading to the displacement or substitution of the bulky TOABr ligands on the NP surface. This process culminates in the formation of a single bilayer. As these iterations were repeated, accumulating up to ten bilayers (referred to as (TOABr-Au NP/TREN)$_{10}$), the formed LbL-assembled Au NP multilayers demonstrated exceptional coverage deposition and an impressive packing density across the entire textile, spanning from its outermost layer to the interior (Figure 3d). This deposition process seamlessly preserved the textile's physical properties and maintained its metallic conductivity (Figure 3e). Similarly, tetraoctylammonium thiosulfate (TOAS)-stabilized Ag NPs have been successfully assembled with NH_2-functionalized linkers such as TAA (note, in this study, TREN is denoted as TAA) using the aforementioned LRR–LbL assembly on commercially available cellulose textiles. This demonstrates their potential utility as a textile current collector and reservoir with the capacity of a substantial mass loading of electrochemically active NPs.[22]

Interestingly, this small molecule linker-mediated LRR–LbL assembly could theoretically imply that a single-molecule linker could bridge adjacent metal NPs at the interfaces, potentially reducing the interparticle distance to the subnanometer scale (Figure 3f).[21,22] Such phenomenon can induce the room-temperature metallic fusion (i.e., sintering) between adjacent metal NPs with low cohesive energy (2.95 eV per Ag atom; 3.81 eV per Au atom), forming a well-connected metallic network. Additionally, the metal NP multilayered films assembled in the organic media exhibited high packing density value about 60% in cubic volume, which could not be achieved in conventional electrostatic interaction LbL assembly in aqueous media (<30%). Consequently, the LRR–LbL-assembled metal NP films exhibited bulk metal-level electrical conductivities even at

thicknesses of only a few hundred nanometers. It is also highly advantageous for maintaining both the structural integrity of the conductive films and the inherent mechanical properties of the pristine textile under continuous mechanical deformation (i.e., bending and crumpling) due to the formation of strong covalent bonds among all components (Figure 3g,h).

2.3.2. LRR–LbL-Induced Electroplating

In general, the LbL assembly processes have been considered to be time consuming due to the significant influence of the number of layers deposited on the desired output performance. Additionally, the LbL process often requires extended adsorption time to achieve the sufficient deposition of each component. Similarly, the electrical conductivity of the LRR–LbL-assembled metal NP film is affected by the layer number, which is directly related to the metal NP content.

As mentioned in the previous section, metal electroplating can produce a well-connected robust metallic layer on the textile surface coated with a conductive seed layer in a relatively short deposition time, ranging from minutes to tens of minutes.[118–121] Since the quality of the conductive seed layer is paramount in the electroplating process, the LRR–LbL-assembled metal NP thin film, which exhibits high electrical conductivity and structural stability even in nanometer-thick layers, may be a promising alternative for forming the conductive seed layer. This possibility has been recently demonstrated by systematically performing the metal electroplating on the LRR–LbL-assembled metal NP layer (i.e., seed layer)-coated textiles.[23–29] In this case, the electrical properties of the seed layer were optimized to achieve a sufficiently low sheet resistance. This optimization allowed for an efficient application of the metal electroplating process by minimizing the number of metal NP layers. As a result, process efficiencies were remarkably improved, ensuring a more effective and streamlined production. For example, Woo et al. reported that various metals (Ni, Cu, and Ag) can be uniformly electroplated onto the various types of textile substrates with only a few layers of only LRR–LbL-assembled tetraoctylammonium (TOA)-stabilized metal NPs (i.e., TOA-Au NPs, TOA-Ag NPs, or TOA-Cu NPs) (**Figure 4**a,b).[23] Specifically, when Ni electroplating was performed onto the LRR–LbL-assembled textile substrates, the resulting textile conductors exhibited an extremely low sheet resistance of $0.08\,\Omega\,sq^{-1}$ and effectively maintained their electrical conductivity even during various forms of mechanical deformation, outperforming Ni-electroless deposited textile conductors (i.e., Ni-ELP) (Figure 4c–e). Importantly, this approach demonstrated approximately seven times faster processing rates and more than three times improved electrical properties, while maintaining a similar thickness of the conductive layer on the textile (approximately 200 nm thick), compared to the LRR–LbL-only process using the same metal NPs (Au NPs).[20] These results hold significant implications, as they not only overcome the efficiency limitations of the LbL assembly method but also offer a promising alternative for fabricating high-quality textile conductors. The integration of this approach with a well-established commercial electroplating technique represents an exciting avenue for the production of advanced textile-based conductors with outstanding performance.
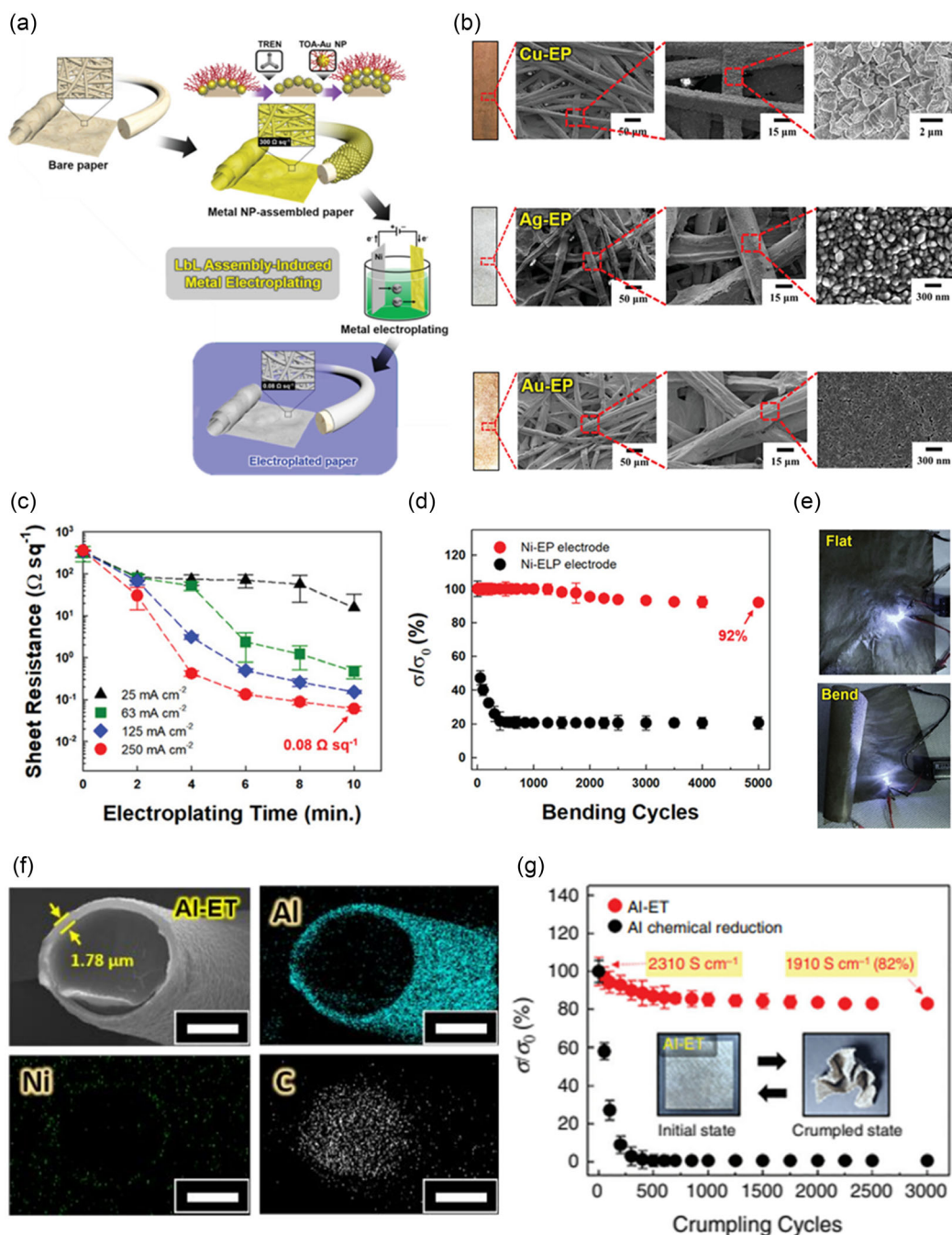
Figure 4. a) Schematic illustration of LRR–LbL-induced metal electroplating for the fabrication of textile conductors. In this process, TOA-stabilized Au NPs were preferentially LbL-assembled with TREN molecules to form a seed layer for electroplating. b) Photographs and FE-SEM images of textile conductors through electroplating of Cu (Cu-EP), Ag (Ag-EP), and Au (Au-EP) onto LRR–LbL-assembled textiles (i.e., (TOA-Au NP/TREN)$_4$-coated textiles). c) Sheet resistance values of textile conductors as a function of Ni electroplating time (min) and external current density (mA cm^{-2}). d) Comparison of the change in electrical conductivity (σ/σ_0) of Ni-EP and Ni-ELP under repeated bending cycle. e) Photographs of Ni-EP textile conductors with an LED connection in flat and bent states. Adapted with permission.[23] Copyright 2021, Wiley-VCH. f) Cross-sectional FE-SEM and EDX mapping images (scale bar, 10 μm) of Al-ETs. g) Comparison of mechanical stability of Al-EP and chemical reduction reaction-based Al textile under repeated crumpling tests. Adapted with permission.[25] Copyright 2021, AIP Publishing.

In addition, the precise electroplating of metals with reliable chemical stability over a wide range of potentials opens up new possibilities for the use of textiles as current collectors in high-energy electrochemical energy storage devices, such as LIBs. To this end, Nam et al. have successfully fabricated high-quality aluminum (Al)-electroplated textile, specifically cotton-based current collectors for LIB cathodes, using the LRR–LbL-assembled metal NP seed (TOA–Au NP, TOA–Cu

**ADVANCED
SCIENCE NEWS**

www.advancedsciencenews.com

**small
structures**

www.small-structures.com

NP, and TOA–Ag NP)-assisted electroplating method in an ionic liquid-based reaction bath.[25] In this case, the choice of an ionic liquid electrolyte was crucial to prevent the formation of a passivating oxide layer (i.e., $Al(OH)_3$) on the pure Al metal surface due to its reaction with water. As a result, the Al-electroplated textile (Al-ET) formed a well-covered, uniform conductive layer (Figure 4f). Remarkably, the Al-ETs exhibited an impressive electrical conductivity and maintained their electrical and structural properties, even under several mechanical deformations like repeated crumpling and bending cycles (Figure 4g). These results were in sharp contrast to Al-textiles prepared by the chemical reduction of Al ions, which suffered a substantial loss of electrical properties after only a few tens of crumpling cycles. The outstanding structural robustness of the Al-ETs can be attributed to the well-defined, strong interfacial interactions between each metal layer (i.e., metal NP-based seed layer, Ni sublayer, and Al layer) and between the seed layer and the textile substrate (as detailed in Section 2.2.2).

These impressive results of the LRR–LbL-induced electroplating approach in the preparation of textile conductors clearly demonstrated the key role of well-designed interfacial structures, achieved through surface chemistry control, in determining the electrical, physical, and mechanical properties of the resulting textile conductors. This approach holds great promise for the development of advanced textile-based conductors with improved performance and durability.

3. Application of Textile Conductor to Energy Electrodes

One of the major advantages of using textile materials (i.e., natural textiles) as current collectors in energy storage systems is the ability to maximize energy density by achieving a higher mass loading of the active components within a limited area/volume of the electrode. This goes beyond simply increasing the amounts of active components per unit area and focuses on optimizing the electrode design to minimize the increase in cell impedance as a function of active layer thickness. This optimization is achieved by the uniform deposition of active components on the surface of textile conductors, which serve as textile current collectors in the following section.[47,98,122–124]

The conventional slurry casting method has long been the standard in producing energy storage electrodes, using commercial metal foils as current collectors. However, this method comes with notable limitations in efficiently utilizing the extensive surface area and porous structure offered by textile substrates. Additionally, the relatively poor mechanical properties (e.g., higher Young's modulus and stiffness) of the thick slurry-cast active layer compared to the textile conductors, together with insufficient interfacial interaction between the active layer and the textile conductor, pose significant challenges in achieving the desired levels of mechanical stability. This issue also contributes to poor electrochemical cycling performance as the active layer is easily delaminated from the textile conductor during lithiation/delithiation process.[125] In addition, the physical mixing of active components, such as carbon-based materials, TMOs, conducting polymers, may not adequately address several structural limitations, including inhomogeneity, agglomeration,

and sedimentation of components within the resulting active layers.[4,126]

It is important to note that incorporation of active components into textile energy electrodes is in line with the previously discussed perspective of introducing conductive components for high-quality textile conductors. In other words, the successful and efficient development of textile energy electrodes requires an appropriate electrode structural design that clearly defines continuous and strong interactions at all interfaces of the newly integrated active layer onto the textile conductors. These considerations have a direct impact not only on the structural integrity of the textile electrodes but also on the charge transfer kinetics at the interfaces within the electrode.

In this context, we further explore the influence of interfacial design on the structural stability and interfacial charge transfer behavior (related to cell impedance) of textile energy electrodes, specifically the assembly of the active layer onto textile conductor, under successive electrochemical sweeps and/or mechanical deformations. Furthermore, we introduce a few important approaches for balancing the high mass loading of active components and high electrical conductivity. It is important to clarify that, unless otherwise specified, the term "textile current collector" in the following sections refers to the "textile conductor" mentioned earlier.

3.1. Interfacial Engineering for Structural Integrity

The lack of strong interfacial adhesion between the active layer and the surface of the textile current collector can lead to serious structural damage such as delamination and cracking when subjected to various mechanical, residual, and/or electrochemical stresses. These problems become more pronounced as the amount of bulky active components increases to achieve higher areal energy densities, further compromising the performance efficiency of the textile energy electrodes.

In terms of tolerance to the various mechanical deformations mentioned earlier, soft materials (e.g., conducting polymers, aromatic organic compounds, metal–organic frameworks (MOF), carbon materials, etc.) with redox-active functional groups coupled with energy storage capability may hold potential as preferred candidates for active components in high-energy textile electrodes, compared to bulky and rigid inorganic active materials.[127–134] Of particular note are the hydrophilic groups present on organic active materials. These groups not only provide excellent dispersion stability in water or polar solvents such as alcohol but also facilitate well-defined interfacial interactions. These interactions include electrostatic attraction and/or hydrogen bonding between the individual electrode components, resulting in robust interfacial adhesion stability.[132,133,135] For example, Wang et al. reported the preparation of flexible solid-state SCs through electrostatic interaction-based spray-LbL assembly.[133] This assembly involved negatively charged graphene quantum dot-reduced graphene oxide (GQD-rGO) and positively charged polyaniline (PANI) (i.e., (GQD-rGO/PANI)$_n$), which were deposited onto commercial carbon fiber cloth (CFC) in aqueous solution (**Figure 5**a). Thanks to the reversible leucoemeraldine-emeraldine-pernigraniline transitions of PANI and the oxygen-containing groups (–OH) on GQD from
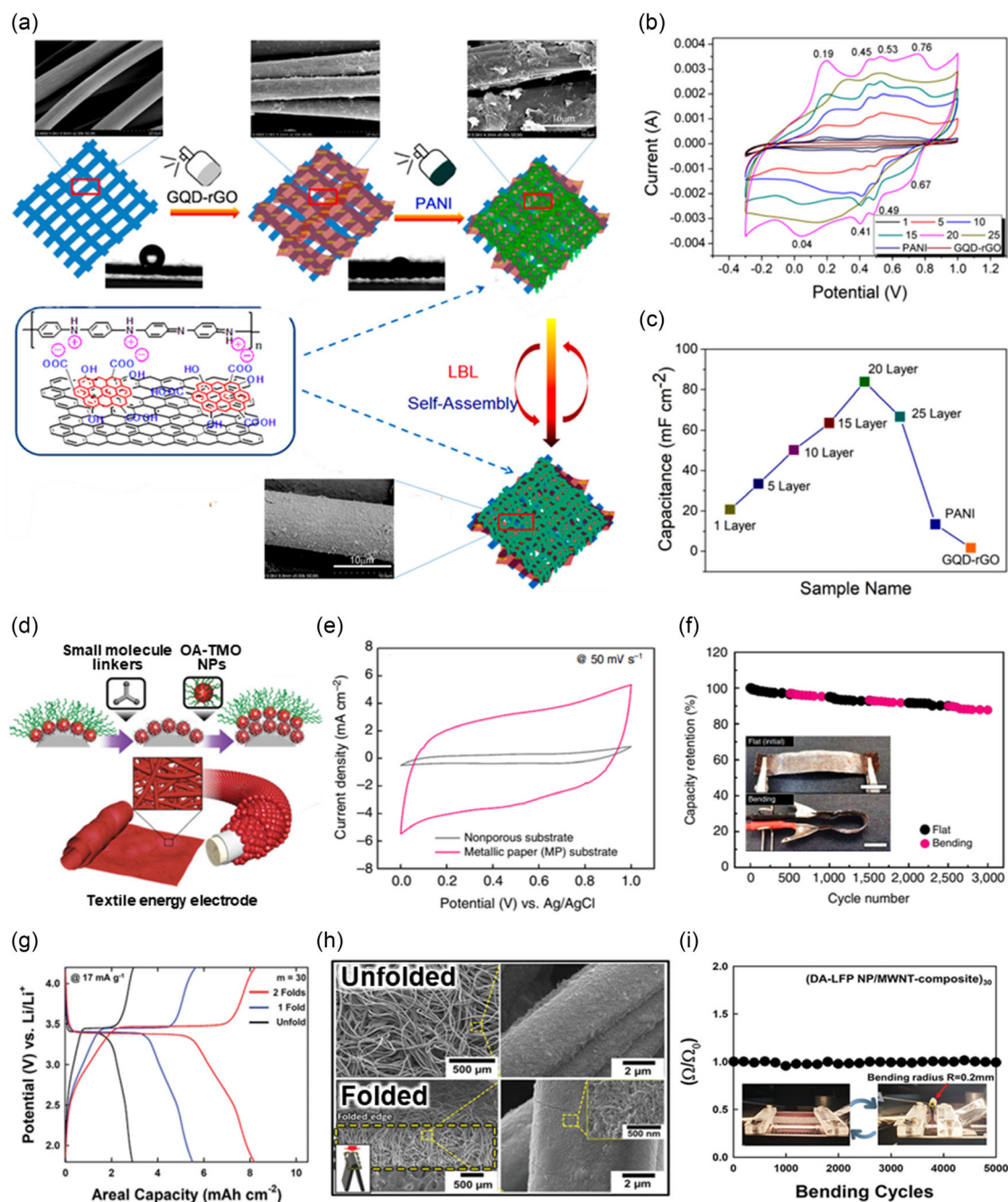
Figure 5. a) Schematic illustration of the preparation of textile energy electrode based on the electrostatic interaction LbL assembly of GQD-rGO and PANI. The FE-SEM images in Figure 5a depict the surface morphology and coating quality of each electrodes. b) CV curves at a scan rate of 50 mV s^{-1} and c) the corresponding maximum areal capacitance (mF cm^{-2}) of (GQD-rGO/PANI)$_n$ ($n = 1$, 5, 10, 15, 20, and 25), PANI, and GQD-rGO composite-based textile energy electrodes. Adapted with permission.[133] Copyright 2019, American Chemical Society. d) Schematic illustration for the preparation of textile energy electrode based on LRR–LbL assembly of OA-TMO NPs and TREN molecules onto textile conductor (i.e., textile current collector). Adapted with permission.[22] Copyright 2021, Wiley-VCH. e) CV curves of metallic paper (MP)- and nonporous (flat) substrate-based textile energy electrodes with same mass loadings of TMO NPs (i.e., MnO NPs) at a scan rate of 50 mV s^{-1}. f) Capacity retention (%) of all-solid-state asymmetric SCs composed with LRR–LbL-assembled textile energy electrodes under repeated mechanical deformation cycles. Adapted under the terms of the CC-BY Creative Commons Attribution 4.0 International license.[20] Copyright 2017, the Authors. Published by Springer Nature. g) Areal capacity (mAh cm^{-2}) of (DA-LiFePO$_4$/MWCNT)-coated textile energy electrodes with different folding numbers. h) FE-SEM images of (DA-LiFePO$_4$/MWCNT)-coated textile energy electrodes at unfolded (top) and folded (bottom) states i) Electrical property (Ω/Ω_0, where Ω_0 indicates a resistance of the initial state before the test) of (DA-LiFePO$_4$/MWCNT)$_{30}$-coated textile energy electrodes under repeated bending cycles. Adapted with permission.[139] Copyright 2021, Wiley-VCH.

the subsequent cyclic voltammetry (CV) redox peaks scanned at 50 mV s^{-1}, the resulting (GQD-rGO/PANI)$_n$-based SCs exhibited a maximum areal capacitance of 82.9 mF cm^{-2} at a current density of 0.1 mA cm^{-2} (Figure 5b). Notably, the performance of the SCs showed a gradual improvement with increasing the number of sprayed layers (n), indicating a close relationship between the energy storage capability and the bilayer number (or loading amounts) of the active layer, referred to as (GQD-rGO/PANI)$_n$ multilayer (Figure 5c). However, it is crucial to acknowledge that during the LbL deposition process, the electrostatic repulsion between identically charged active components limits the loading amounts of active components per layer. This limitation results in a significant need for a large number of bilayers, leading to inefficiencies and time-consuming efforts to achieve the desired high energy density for SCs. Moreover, further increase in the bilayer number ($n > 20$) leads to dense and nonuniform film deposition with partial agglomeration of the charged components, which can be observed in the electrostatic attraction-induced LbL assembly of particulate materials.[136,137] This phenomenon can not only hinder fast and efficient ion (electrolyte) penetration into the interfaces but also result in poor structural stability.

As discussed in a previous section, the LRR–LbL assembly method offers a solution by enabling the formation of robust thin films consisting of uniformly and densely packed active component arrays that effectively cover the entire exposed surface of the textiles through well-defined interfacial interactions. Importantly, this assembly approach can be readily applied to various high-energy TMO NPs (e.g., RuO$_2$, MnO$_2$, Fe$_3$O$_4$, Co$_3$O$_4$, LiFePO$_4$, etc.), allowing for the sequential deposition of high-quality active layers onto the LRR–LbL-assembled textile conductors without causing significant structural damages or interfacial mismatches. This was systematically demonstrated by successfully integrating high-energy TMO NPs, such as manganese oxide (MnO) NPs or magnetite (Fe$_3$O$_4$) NPs, into LRR–LbL-assembled textile current collectors *via* the same ligand replacement mechanism (Figure 5d).[20,22,23] In this process, the high-crystalline TMO NPs stabilized by bulky oleic acid (OA) were LbL-assembled with NH$_2$-functionalized small-molecular organic linkers in organic media through strong covalent bonding. During this assembly, the native hydrophobic ligands on the TMO NP surface were replaced by the NH$_2$ groups of the small molecule linkers, resulting in the formation of densely packed thin-film structures with numerous nanopores between neighboring NPs. Interestingly, the LRR–LbL-assembled TMO NP arrays exhibited significantly high mass densities comparable to a random close packing density ($\approx$64%) for identical spherical solids in a cubic volume.[138] As a result, the LRR–LbL-assembled pseudocapacitive TMO NP layer-based textile SCs demonstrated superior specific capacitances compared to nonporous flat substrate-based electrodes (Figure 5e), with excellent capacity retention of over 90% of the initial values after 5000 cycles, regardless of the mass density of TMO NPs. Furthermore, the all-solid-state asymmetric SCs systems composed of MnO NP- and Fe$_3$O$_4$ NP-based textile energy electrodes effectively maintained their electrochemical performance up to $\approx$90% even under thousands of consecutive bending deformations, demonstrating the excellent structural integrity of the LRR–LbL-assembled films (Figure 5f).

One of the ultimate challenges for textile-based energy electrodes (or conductors) is whether their electrical and/or electrochemical properties can be reliably maintained even under extremely harsh mechanical stresses such as fully folded or crumpled states with sharp edge curvatures, which are likely to occur in everyday life. Kwon et al. fabricated a textile-type LIB cathode by the LRR–LbL assembly between dioleamide-stabilized lithium iron phosphate (DA-LiFePO$_4$) NPs and NH$_2$-functionalized MWCNTs, which could be increased proportionally with the increase in the folding number without noticeable changes in the electrochemical overpotential (Figure 5g).[139] These results were mainly attributed to the structural stability of the LRR–LbL-assembled LiFePO$_4$ NP composite layer, which exhibited no mechanical delamination or cracks even in a fully folded state (Figure 5h), and also showed stable electrical properties even after 5000 repeated bending cycles (Figure 5i). This was in stark contrast to the slurry-cast textile electrode, which showed very poor interfacial adhesion behavior.

The LRR–LbL assembly technique provides an intriguing platform to effectively exploit the physical nature of the pristine textiles in the preparation of textile energy electrodes, but the folded layer number-dependent behavior on the output performance is one of the challenges that should be addressed for practical applications. Although the simple folding approach can greatly increase energy storage performance in a limited electrode area, the thickened electrode thickness, mainly due to the textile itself, can lead to mechanical flexibility problems.

Recently, Yong et al. have reported an electrochemically active textile current collector (i.e., EP Cu-textile) for LIB anodes by hydrogen-bonding/LRR–LbL assembly-induced Cu electroplating on a commercially available cotton textiles (**Figure 6**a).[29] Specifically, Au NP-MWCNT multilayers were preferentially deposited onto the cotton textiles, which was converted into the conductive textile suitable for Cu electroplating (Figure 6b). After this Cu electroplating process, all components within the textile electrode (i.e., electroplated Cu layer, Au NP seed layer, MWCNT multilayer, and cotton textile) were strongly assembled through well-defined interfacial interactions involving hydrogen bonding and covalent bonding. Additionally, this study highlights that the Cu electroplating method under mild conditions yields a high-quality Cu layer with a partially oxidized CuO$_x$ thin layer on the conductive textile. This unique combination enhances electrochemical performance and durability, presenting a notable contrast to chemical reduction-induced Cu textiles (CR Cu-textile), as depicted in Figure 6c–f. Furthermore, these results strongly suggest that the EP Cu-textile can serve as an excellent current collector for incorporating energy materials such as lithium titanate (Li$_4$Ti$_5$O$_{12}$, LTO), which is used as a LIB anode material. Additionally, it possesses energy reservoir properties, allowing it to function as the textile energy electrode itself. Remarkably, this dual functionality of a textile in an energy storage device has not been reported previously.

The authors described this phenomenon as a result of the synergistic effect between 1) the reversible formation/dissolution of polymeric gel-like phase promoted by well-dispersed copper oxide NPs and 2) the newly formed flower-like 3D structure during continued GCD cycling (Figure 6g). These results evidently demonstrate that the fine control of the interfacial interactions existing between different electrode components has significant
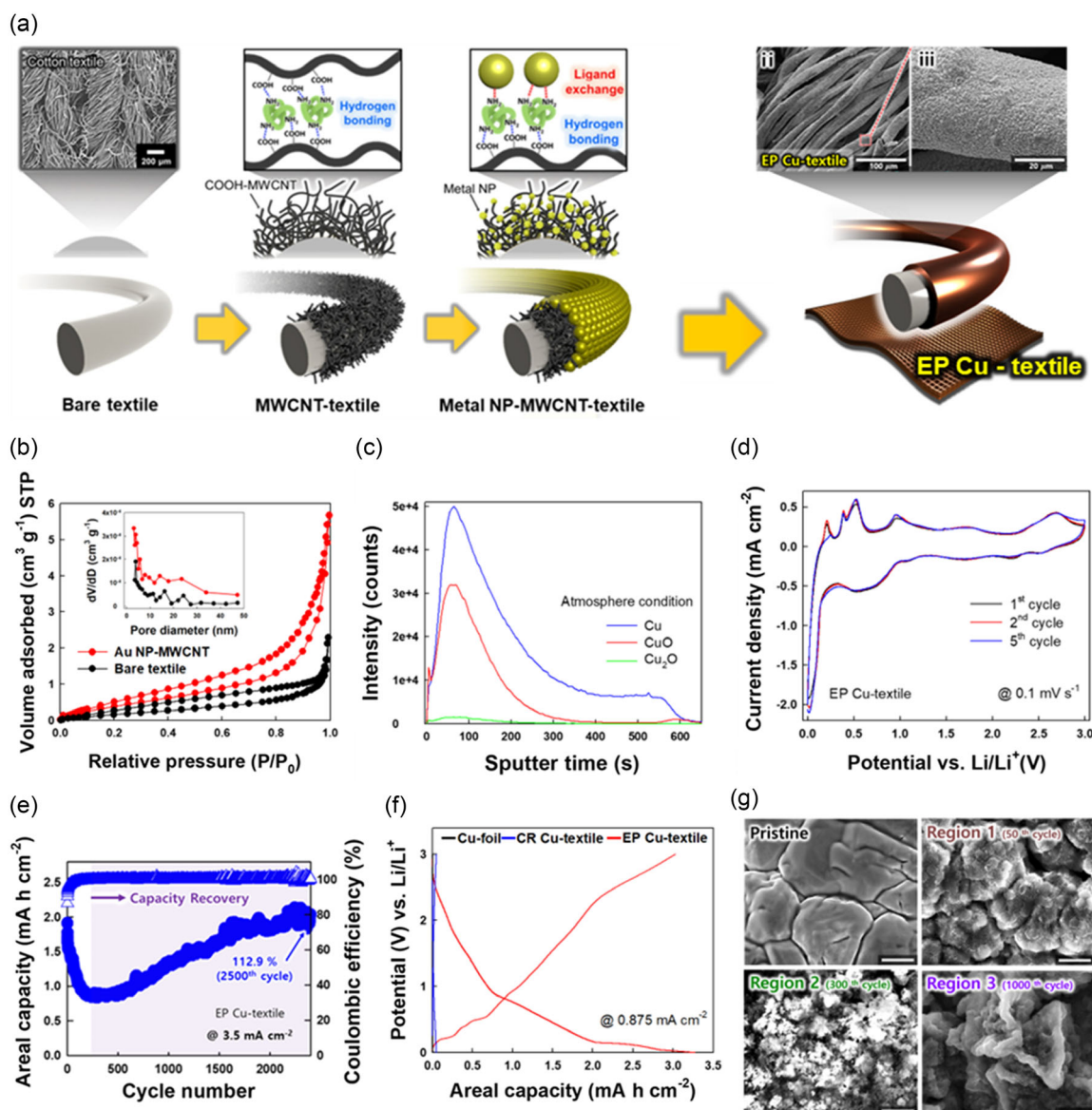
Figure 6. a) Schematic illustration for the preparation of an electrochemically active textile current collector for LIB anodes through hydrogen-bonding/LRR LbL assembly-induced Cu electroplating process onto a commercially available cotton textile. The FE-SEM images show surface morphology of each textile. b) Comparison of specific surface area between the TOABr-Au NP/(COOH-MWCNT/TREN)$_5$-coated textile (Au NP-MWCNT) bare textiles and the bare textile through the Brunauer Emmett–Teller (BET) method. c) Time-of-flight secondary ion mass spectrometry (TOF-SIMS) profile of Cu-electroplated/Au-sputtered Si wafer prepared from thermal annealing under atmosphere conditions. Suggesting a partially oxidized outermost thin layer (CuO/Cu$_2$O mixture) on the prepared textile conductor. d) CV curves of EP Cu-textile at a scan rate of 0.1 mV s^{-1}. e) Cycling stability and coulombic efficiency (%) of EP Cu-textile at a current density of 1.75 mA cm^{-2}. f) Areal capacity (mA h cm^{-2}) of EP Cu-textile, CR Cu-textile and Cu-foil at 0.875 mA cm^{-2}. g) FE-SEM images of EP Cu-textile after various GCD cycles (scale bar, 500 nm). Adapted with permission.[29] Copyright 2023, Elsevier.

effect on the mechanical stability and energy storage performance of textile electrodes.

3.2. LRR–LbL Design for Improving Interfacial Charge Transfer Kinetics

Energy storage systems face a critical dilemma between energy and power efficiency. While 3D-structured textile current collectors offer higher mass loading of high-energy active components,

resulting in increased areal energy density compared to conventional metal foil-based systems,[140] the sluggish charge transfer kinetics between neighboring active components with poor electrical conductivity remains a significant obstacle to achieving the desired energy storage performance. To overcome this challenge, it is essential to achieve a uniform deposition of an active layer with well-defined charge transfer pathways.

In general, conventional methods such as hydrothermal, solvothermal, or electroless plating have been used to chemically grow active components onto textile current collectors, resulting
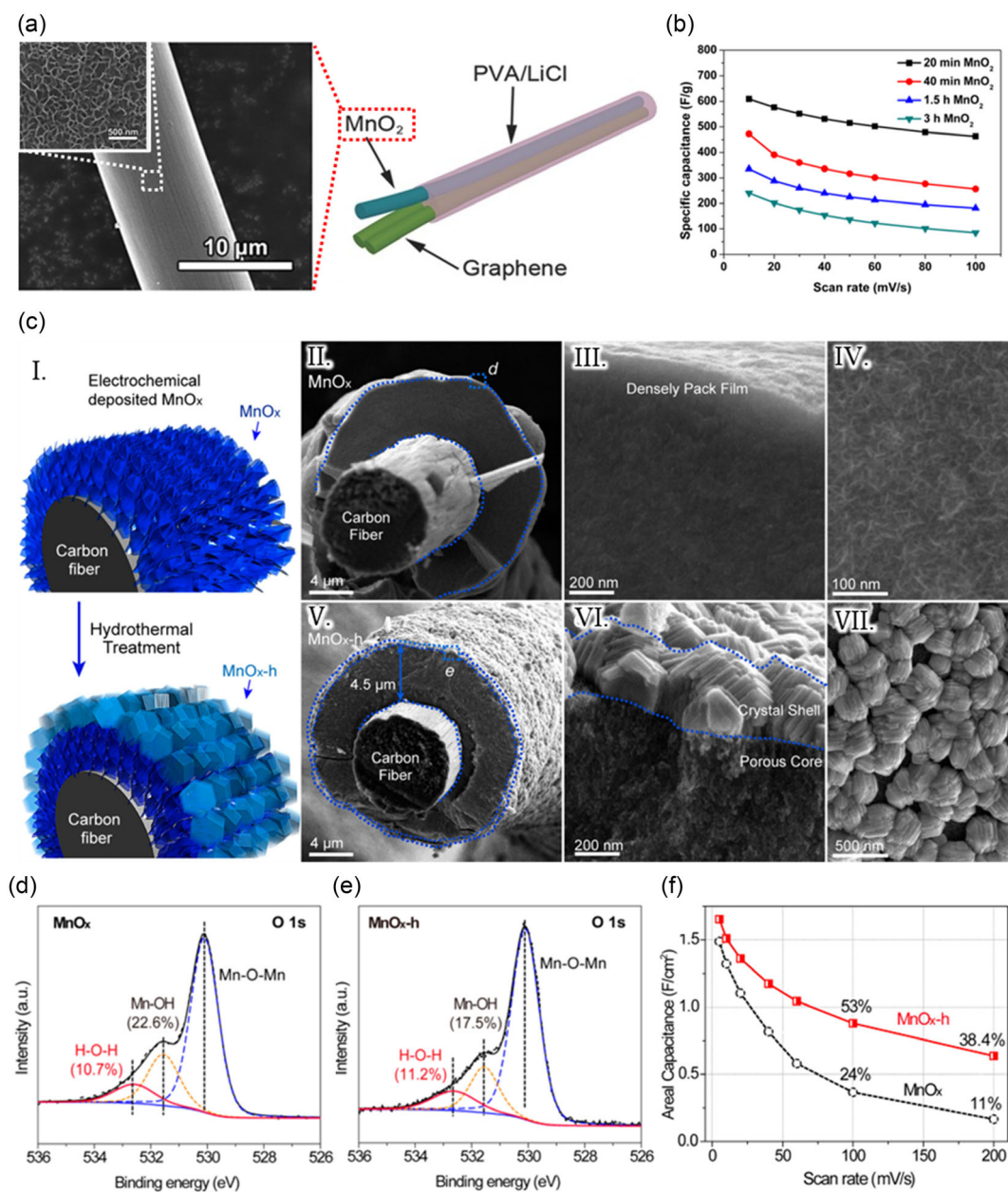
**ADVANCED
SCIENCE NEWS**

www.advancedsciencenews.com

**small
structures**

www.small-structures.com

Figure 7. a) Schematic illustration of all-solid-state SCs composed of MnO_2 (cathode)- and graphene (anode)-coated carbon fibers. The FE-SEM images show MnO_2 nanosheet-coated carbon fiber prepared through hydrothermal growth of MnO_2 nanosheets on the carbon fiber surface b) Scan rate ($mV\,s^{-1}$)-dependent specific capacitance ($F\,g^{-1}$) of MnO_2/carbon fiber electrodes with different mass loading of MnO_2. Adapted with permission.[143] Copyright 2015, Wiley-VCH. c) Schematic illustration and FE-SEM images of manganese oxide (MnO_x and MnO_x-h) film-coated carbon fibers. Deconvoluted O 1s XPS spectra of d) MnO_x and e) MnO_x-h. f) Scan-rate dependent areal capacitance ($F\,cm^{-2}$) of MnO_x- and MnO_x-h-based textile electrodes. Adapted with permission.[144] Copyright 2017, American Chemical Society.

in the creation of a well-covered, thin active composite layer.[141–144] In a study presented by Yu et al. MnO_2 nanosheet-coated carbon fiber electrodes were fabricated using a hydrothermal technique and then integrated into all-solid-state asymmetric SCs along with graphene-coated carbon fiber-based negative electrodes (**Figure 7**a).[143] To achieve this, the carbon fibers were pretreated by immersion in hydrochloric acid. This treatment facilitated the adsorption of hydrogen and

chloride ions, which served as nucleation and growth sites for MnO_2 nanosheets. The growth of MnO_2 nanosheet arrays on the carbon fibers was uniform and perpendicular (see the FE-SEM image inset in Figure 7a). This unique arrangement promoted rapid electron transfer and ion diffusion kinetics, consequently enabling high specific capacitance of $634.5\,F\,g^{-1}$ at current density of $2.5\,A\,g^{-1}$ (Figure 7b) and remarkable capacity retention about 99% even after 3000 GCD cycles, and mechanical

ADVANCED
SCIENCE NEWS

www.advancedsciencenews.com

small
structures

www.small-structures.com

stability. However, as shown in Figure 7b, it is worth noting that intrinsically poor electrical conductivity of MnO_2 can impede its effective activation, leading to a marked reduction in the output performance of the SCs as the loading amount (i.e., reaction time) of MnO_2 increases. This limitation becomes particularly evident in terms of rate capability, especially as the loading amount of MnO_2 nanosheets on carbon fiber increases from 0.12 to 1.1 mg cm^{-2} (this loading amount corresponds to an increase in layer thickness from 58.5 to 318.7 nm). On the other hand, the excessively low loading amount of the active components may prove insufficient for energy storage applications that require practical performance.[145,146]

Furthermore, since the electrical conductivity and ion diffusion kinetics of most TMO NPs are strongly influenced by their crystallinity and stoichiometry,[147–149] it is desirable to minimize the presence of nonstoichiometric amorphous species during TMO synthesis. A few years ago, Li group introduced a hydrothermal treatment approach that could exploit Ostwald ripening-induced structural modification on an amorphous MnO_x film-coated carbon cloth (Figure 7c).[144] As confirmed by O 1s X-ray photoelectron spectroscopy (XPS) spectra, the peak area of MnO_x-h (Figure 7d) was smaller than that of MnO_x (Figure 7e) at the binding energy of 531.5 eV (Mn–O–H), indicating the formation of a highly crystalline outermost MnO_x-h shell layer with the low content of nonstoichiometric manganese oxides (e.g., trivalent Mn species). Furthermore, due to the improved electrical conductivity, a significant improvement in capacitive performance was observed, with an areal capacitance of 1610 mF cm^{-2}, even at a high mass loading of 9 mg cm^{-2} (Figure 7f).

Another effective way to fabricate the textile energy electrodes is to deposit as-synthesized highly crystalline energy nanomaterials, such as TMO NPs, onto highly porous textile current collectors composed of numerous conductive fibrils.[4,150–152] However, the application of TMO NP-based textile electrodes has introduced a new issue that requires proper interfacial design for facile charge transfer due to increased specific surface area and interfaces. In particular, the presence of polymeric ligands and linkers on the surface of TMO NPs can act as insulating barriers that hinder the access and transfer of charge carriers (electrons and ions) at the interfaces of adjacent electrode components, such as current collector/TMO NP, TMO NP/TMO NP, and TMO NP/electrolyte.[153–155] Therefore, a crucial strategy for achieving high-performance textile energy electrodes with densely packed TMO NP arrays lies in the ligand-controlled interfacial design of TMO NPs.

The effect of the ligands attached to the TMO NP surface on the charge transfer kinetics in the TMO NP arrays is highly dependent on various properties, such as molecular structure, type and arrangement of functional groups, and chain length.[28,156–158] For example, replacing the bulky OA ligand on semiconducting Fe_3O_4 NP surface with a smaller organic molecular linker (i.e., TREN with $M_w \approx 146$ g mol^{-1}) resulted in a remarkable improvement of the electrical properties by more than 1000-fold, inducing a transition from insulating to semiconducting behavior in the ≈200 nm-thick solid-state thin film.[159] Considering that the electrical conductivity or electrochemical property of active components significantly influences the output performance of energy storage electrodes, these results strongly

suggest that ligand engineering-mediated assembly, such as LRR–LbL assembly of TMO NPs, may serve as an effective solution for fabricating high-performance textile energy electrodes.

This possibility had been systematically investigated through high-energy TMO NP (i.e., OA and/or oleylamine (OAm)-Fe_3O_4 NP)-based SCs that were prepared by LRR–LbL assembly using different types of linkers.[28] As a comparison, two carboxylic acid (COOH)-functionalized linkers with different molecular weights were used: Mn (II)-porphyrin bis-carboxylic acid (MnPP, $M_w \approx 931$ g mol^{-1}), which is electrochemically active and exhibits semiconducting properties due to its unique chemical structure, and insulating poly(acrylic acid) (PAA, $M_w \approx 450\,000$ g mol^{-1}). During the LbL deposition process, the COOH group of each organic linkers exhibited high interfacial affinity,[160–162] facilitating multidentate binding with the TMO NP's surface and replacing the insulating native ligands (OA/OAm) of the TMO NP. As shown in **Figure 8**a, the relaxation time constant of MnPP was much lower than that of the PAA linker.[163] However, the electrical property of semiconducting MnPP was further enhanced by incorporating additional conductive NPs such as indium tin oxide (ITO) NPs (Figure 8b). The resulting electrochemically active MnPP linker-based textile-type SCs (MnPP-TCCs) exhibited uniform coating of all active components on the textile (Figure 8c). Additionally, it showed significantly improved areal capacitance (≈0.80 F cm^{-2} at 50 mA cm^{-2}) and rate capability compared to the insulating PAA linker-based electrodes (PAA-TCCs, ≈0.13 F cm^{-2}), despite having the same mass loading of TMO NPs (≈9.8 mg cm^{-2}) (Figure 8d). These notable results can be attributed to the enhanced charge transfer kinetics and electrochemical activity resulting from the ligand replacement with redox-active MnPP linkers, which have a lower molecular weight than PAA.

The versatility of the LRR–LbL assembly, applicable to various metal and metal oxide NPs, has led to a breakthrough in effectively reducing and controlling the cell impedance caused by the mass loading of TMO NPs.[20,28,153,164,165] Specifically, the integration of conductive NPs, such as Au NPs or ITO NPs, through strong covalent bonding with small molecular linkers in an alternating LbL deposition of energy TMO NPs and conductive NPs, has been proposed.[25,28,153,165] This approach provides better electrical conductivity compared to organic conductivity enhancers, enabling efficient upscaling of energy storage performance by mass loading of TMO NPs. For instance, periodic deposition of conductive ITO NP layers between pseudocapacitive MnO NP layers through multidentate small linker (tricarballylic acid, TC, $M_w \approx 176$ g mol^{-1})-mediated LRR–LbL assembly significantly reduces cell impedance, resulting in improved energy storage performance and efficiency compared to MnO NP-based SCs electrodes without ITO NP layers in the same total mass loading.[165] In this case, the inserted ITO NP layers serve as well-connected electron pathways, facilitating electron transfer over the entire electrode area and minimizing the presence of inactive dead mass/volume in the electrodes.

A recent study by Song et al. reported a COOH-functionalized carbon nanocluster (CCNs)-mediated LRR–LbL assembly for binder-free textile-type LIB anodes.[166] In this process, conductive CCNs were directly LbL-assembled with Fe_3O_4 NPs stabilized by hydrophobic ligands (OA/OAm) without additional binders (Figure 8e). The ligand-replacement-reaction-induced
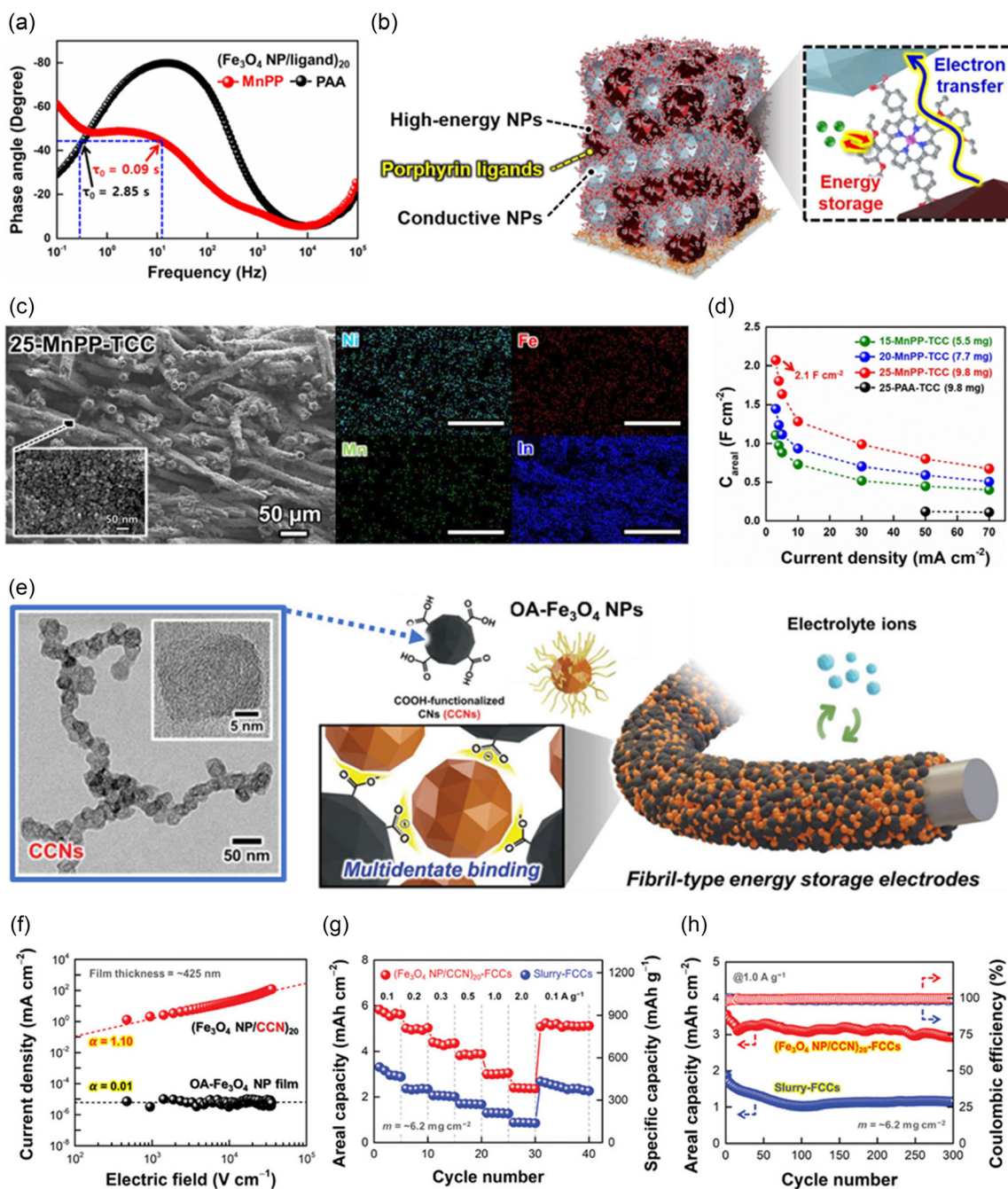
Figure 8. a) Phase angle of Bode plots for $(Fe_3O_4/MnPP)_{20}$ and $(Fe_3O_4/PAA)_{20}$ electrodes from electrochemical impedance spectroscopy (EIS) measurements. b) Schematic illustration of the multilayers composed of high-energy NPs (OA-Fe_3O_4 NPs), conductive NPs (OAm-ITO NPs), and porphyrin ligands (MnPP linkers). c) Cross-sectional FE-SEM and the corresponding EDX mapping images of MnPP-TCC. d) Areal capacity (F cm^{-2}) at various current density (mA cm^{-2}) according to the type of linkers (i.e., MnPP and PAA). Adapted with permission.[28] Copyright 2023, Elsevier. e) Schematic illustration of a carboxylic acid (COOH)-functionalized carbon nanoclusters (CCN)-mediated LRR–LbL assembly for binder-free textile-type Fe_3O_4 NP-based LIB anodes and high-resolution transmission electron microscopy (HR-TEM) image of CCN. f) Comparison of ohmic conduction behaviors of LRR–LbL-assembled CCN/Fe_3O_4 NP nanoblends and slurry-cast OA-Fe_3O_4 films under an externally applied electric field. g) Comparison of areal/specific capacities with varying current densities and h) cycling stability between (CCN/Fe_3O_4 NP)-FCCs and slurry-casted electrodes. Adapted with permission.[166] Copyright 2023, Wiley-VCH.

multidentate binding between the COOH groups of CCN and the Fe_3O_4 NP surface effectively removed the native bulky ligands (OA/OAm). The LRR–LbL-assembled CCN/Fe_3O_4 NP

nanoblends exhibited ohmic conduction behaviors under an externally applied electric field, in contrast to slurry-cast OA-Fe_3O_4 films, which showed insulating properties

(Figure 8f). In addition, the oxygen-containing groups (COOH) on the surface of the CCNs contributed to the overall capacities of the textile energy electrode through a reversible Faradaic reaction with lithium ions.[167,168] Consequently, the conductive CCNs acted as active linkers, resulting in textile-type LIB anodes (i.e., (CCN/Fe$_3$O$_4$ NP)–FCCs) with a maximum areal capacity of $\approx$5.67 mA h cm^{-2} at 0.1 A g^{-1} with good rate capability and cycle retention, outperforming slurry-cast electrodes (Figure 8g,h).

The interfacial structure plays a crucial role in influencing the charge (electron and ion), transfer efficiency, and structural integrity among all electrode components with the same or different phases. In the context of textile-based electrodes, which require specific levels of mechanical and structural stability, the establishment of well-defined, strong interfacial interactions between each electrode component is essential. Additionally, we have explored the LRR–LbL assembly method for textile electrodes, comparing it to conventional approaches that primarily rely on depositing active components through either physical or chemical methods. Within this framework, we delved into the pivotal aspect of interfacial design, highlighting the critical importance of accurately defining the interfacial interactions between each electrode component and improving the kinetics of charge transfer. The reported results clearly indicate that the efficient use of textiles is highly dependent on the appropriate modulation of interfacial conditions between the extremely large surface area of the textile and the functional materials deposited thereon, which affects the electrochemical performance of the fabricated textile energy electrodes (**Table 1** and **2**).[20,22,23,25,26,28–30,139,166,169–186]

4. Conclusion and Perspective

The incorporation of conductive and electrochemically active components into a 3D porous structured textile, composed of numerous fibrils, holds great promise. The application, performance, and operational stability of various electrochemical textile electrodes, including SCs and LIBs, depend on factors such as the type and loading amounts of conductive and active components, the interfacial interactions between these components, and the mechanical flexibility of the resulting electrodes. Particularly, considering that the areal energy performance

Table 1. Electrochemical performances comparison of textile-based SC electrodes.

Textile conductor	Active material [mass loading]	Method	Electrochemical performance	Cycling retention	References
LbL-assembled Au NPs	MnO/Au NP (4.09 mg cm^{-2})	LRR–LbL	1350 mF cm^{-2} (@5 mV s^{-1})	91.3% after 5000 cycles (@100 mV s^{-1})	[20]
LbL-assembled Ag NPs	Fe$_3$O$_4$	LRR–LbL	212 mF cm^{-2} (@5 mV s^{-1})	96.7% after 5000 cycles (@100 mV s^{-1})	[22]
LbL-assisted Ni Electroplating	MnO/Au NP (4.18 mg cm^{-2})	LRR–LbL	1710 mF cm^{-2} (@5 mV s^{-1})	86.1% after 5000 cycles (@100 mV s^{-1})	[23]
LbL-assisted Ni Electroplating	NiCo LDH (5.12 mg cm^{-2})	Electroplating	12 200 mF cm^{-2} (1-stack) (@10 mA cm^{-2}) 28 800 mF cm^{-2} (3-stack) (@30 mA cm^{-2})	82.2% after 10 000 cycles (@20 mV s^{-1})	[26]
LbL-assisted Ni Electroplating	Fe$_3$O$_4$ NP/MnPP/ITO NP/MnPP (9.8 mg cm^{-2})	LRR–LbL	2100 mF cm^{-2} (@3 mA cm^{-2})	88% after 5000 cycles (@0.5 mA cm^{-2})	[28]
rGO dip-coating	PANI/rGO (3.14 mg cm^{-2})	Polymerization	1221 mF cm^{-2} (@1 mA cm^{-2})	94.4% after 10 000 cycles (@30 mA cm^{-2})	[169]
PPy Polymerization	PPy (53 mg cm^{-2})	Polymerization	4848 mF cm^{-2} (@1 A cm^{-2})	88% after 5000 cycles (@50 mV s^{-1})	[170]
Carbon Cloth	MnO2 (10 mg cm^{-2})	Electroplating	3040 mF cm^{-2} (@ 3 mA cm^{-2})	108% after 2000 cycles (@40 mA cm^{-2})	[171]
Ni electroless plating	NiCo-LDH/NS [a] (1.77 mg cm^{-2})	Hydrothermal/electroplating	1147 mF cm^{-2} (@3 mA cm^{-2})	92% after 2000 cycles (@12 mA cm^{-2})	[172]
Carbon Cloth	PANI/ZIF-67 (4 mg cm^{-2})	Electroplating/slurry casting	2146 mF cm^{-2} (@10 mV s^{-1})	–	[173]
rGO dip-coating	MXene/rGO (1.8 mg cm^{-2})	Spray-coating	258 mF cm^{-2} (@5 mV s^{-1})	–	[174]
Graphene dip-coating	MnO$_2$/Graphene (0.805 mg cm^{-2})	Hydrothermal	332 F g^{-1} (@2 mV s^{-1})	>100% after 1000 cycles (@0.8 mA cm^{-2})	[175]
Carbon textile	ZnS (1.22 mg cm^{-2})	Hydrothermal and annealing	747 F g^{-1} (@5 mV s^{-1})	–	[176]
Ag sputtering	Fe(Ni)Co$_2$S$_4$ (2.3 mg cm^{-2})	Hydrothermal	3500 mF cm^{-2} (@5 mA cm^{-2})	95% after 5000 cycles (@5 mA cm^{-2})	[177]
Carbon Cloth	rGO + CNT (1.8 mg cm^{-2})	Slurry casting	129 F g^{-1} (0.1 A g^{-1})	–	[178]

[a] NS: Nanosheets.

Table 2. Electrochemical performances comparison of textile-based LIBs electrodes.

Textile conductor	Active material (mass loading)	Method	Electrochemical performance	Cycling retention	References
Carbonization/Ni electroplating	Fe_3O_4 (5.3 mg cm^{-2})	LRR–LbL	5.67 mA h cm^{-2} (1-stack) 11 mA h cm^{-2} (2-stack) (@0.1 A g^{-1})	82.5% after 300 cycles (@1.0 A g^{-1})	[166]
LbL-assembled MWCNT	$LiFePO_4$ (15.2 mg cm^{-2})	LRR–LbL	2.9 mA h cm^{-2} (@17 mA g^{-1})	92.1% after 300 cycles (@170 mA g^{-1})	[139]
LbL-assisted Al electroplating	$LiFePO_4$ (8 mg cm^{-2})	LRR–LbL	1.07 mA h cm^{-2} (@0.1 C)	87.1% after 580 cycles (@1 C)	[25]
LbL-assisted Cu electroplating	$Li_4Ti_5O_{12}$ (10 mg cm^{-2})	Vacuum filtration/doctor blading	4.2 mA h cm^{-2} (@0.875 mA cm^{-2})	80.1% after 500 cycles (@1.75 mA cm^{-2})	[29]
Ag NW spray coating	$Li_4Ti_5O_{12}$ (5 mg cm^{-2})	Ultrasonic spray	3.2 mA h cm^{-2} (fourfolded) (@1 C)	≈99% after 1000 cycles (@1 C)	[30]
Cotton textile	Fe_3O_4 (−)	Dyeing/carbonization	3.55 mA h cm^{-2} (@0.1 mA cm^{-2})	91.5% after 100 cycles (@1 mA cm^{-2})	[179]
CNT dip coating	$Li_4Ti_5O_{12}$ (145 mg cm^{-2})	Soaking	23.5 mA h cm^{-2} (@0.1 C)	>90% after 350 cycles (@0.1 C)	[180]
CNT dip coating	$LiCoO_2$ (≈1 mg cm^{-2})	Doctor blading	122 mA h g^{-1} (@25 mA g^{-1})	85% after 17 cycles (@25 mA g^{-1})	[181]
Carbonization	MoS_2 (4.4 mg cm^{-2})	Hydrothermal	5.3 mA h cm^{-2} (@0.5 mA cm^{-2})	91% after 50 cycles (@0.5 mA cm^{-2})	[182]
N-doped carbonization	VN[a] (≈2.5 mg cm^{-2})	Solvothermal and annealing	5.3 mA h cm^{-2} (@0.1 mA cm^{-2})	0.65 mA h cm^{-2} after 400 cycles (@5 mA cm^{-2})	[183]
Ni electroless deposition	V_2O_5 HoMS[b] (2.5 mg cm^{-2})	Doctor-blading	271.2 mA h g^{-1} (@200 mA g^{-1})	≈55% after 500 cycles (@200 mA g^{-1})	[15]
Ni electroless/Au galvanic replacement	CuS (≈1 mg cm^{-2})	Electroless deposition/ sulfurization	583 mA h g^{-1} (@0.5 C)	≈68.6% after 300 cycles (@0.5 C)	[184]
Carbonization	Fe_3O_4@RGO (0.7 mg cm^{-2})	Hydrothermal/electrostatic assembly	1058 mA h g^{-1} (@0.5 A g^{-1})	109% after 2000 cycles (@0.5 A g^{-1})	[185]
Carbonization	$Li_4Ti_5O_{12}$ (1.5 mg cm^{-2})	Hydrothermal	162 mA h g^{-1} (@1 C)	99% after 1000 cycles (@50 C)	[186]

[a]VN: Vanadium nitride. [b]HoMS: Hollow multishelled structures.

values of energy storage electrodes serve as practical performance indicators, the importance of textile energy electrodes and their applications is expected to deepen and expand.

In order to achieve the successful development of highly conductive textile conductors and the resulting textile energy electrodes, certain key strategies are essential. First, minimizing the loading amount of insulating and electrochemically inactive components, such as bulky organic ligands, linkers, and/or polymeric binders, is crucial. Second, the conformal deposition of conductive and active components onto textile fibrils is necessary. Third, ensuring favorable interfacial interactions between electrode components is essential.

While metal NPs themselves exhibit high electrical conductivity and hold promise as conductive components for textile energy electrodes, the presence of numerous contact resistance (arising from the separation distance between metal NPs) significantly hampers the overall electrical conductivity of metal NP-incorporated electrodes (including textile current collector). Additionally, if there is no favorable interfacial interaction between metal NPs and active components, these issues may be exacerbated. Furthermore, the complex synthesis and challenging mass production of metal NPs diminish their commercial viability. These shortcomings also apply to metal NWs,

despite their ease of electrical connection. Taking these considerations into account, it appears that, instead of pristine hydrophobic CNTs or conducting polymers, the unique CNTs or conducting polymers modified with interfacial interaction groups and possessing higher electrical conductivity may present the most promising candidates among various conductive components.

Although LbL assembly approaches such as hydrogen-bonding-, electrostatic interaction-, or ligand replacement reaction-based LbL assemblies enable the conformal coating of functional components (i.e., conductive and active components) onto textile fibrils through reciprocal interfacial interactions, they can be time consuming and limit the diversity, versatility, and commercial applications of textile electrodes. However, these issues can be optimized by simply controlling the concentration of solution and expanding the following assembly by automatic spray deposition or roll-to-roll process, which will further allow the production of industrial-grade conductor and/or energy electrodes.[103] Moreover, the adoption of an LbL assembly-induced electroplating approach can significantly alleviate these drawbacks, resulting in the preparation of high-quality textile conductors/electrodes with bulk metal-like electrical conductivity, extremely large surface area, high flexibility, light weight,

and exceptional electrochemical performance. The combination of ligand replacement-induced interfacial design of electrode components with commercial metal electroplating can be a breakthrough in overcoming barriers to the use of textile electrodes in practical energy storage devices. As a result, this combined approach holds immense potential for various wearable/portable electrochemical devices, including energy conversion and biomedical devices, as well as energy storage devices. Therefore, we envision that such an approach can be widely and effectively applied to the electrical conductors and energy storage electrodes for various wearable/portable electrochemical devices, including energy conversion and biomedical devices as well as energy storage devices.

Conflict of Interest

The authors declare no conflict of interest.

Author Contributions

W.C. and E.Y. contributed equally to this work. W.C., E.Y., Y.K., Y.J.C., and J.C. wrote and revised the manuscript. All authors discussed the results and commented on the manuscript.

[1] H. Cha, J. Kim, Y. Lee, J. Cho, M. Park, *Small* **2018**, *4*, 1702989.

[2] Y. Ko, S. Lee, C. H. Kwon, S. W. Lee, J. Cho, *Adv. Energy Mater.* **2021**, *11*, 2002969.

[3] R. H. Terrill, T. A. Postlethwaite, C.-H. Chen, C.-D. Poon, A. Terzis, A. Chen, J. E. Hutchison, M. R. Clark, G. Wignall, J. D. Londono, R. Superfine, M. Falvo, C. S. Johnson Jr., E. T. Samulski, R. W. Murray, *J. Am. Chem. Soc.* **1995**, *117*, 12537.

[4] Y. Ko, C. H. Kwon, S. W. Lee, J. Cho, *Adv. Mater.* **2020**, *32*, 2001924.

[5] C. H. Kwon, Y. Ko, D. Shin, M. Kwon, J. Park, W. K. Bae, S. W. Lee, J. Cho, *Nat. Commun.* **2018**, *9*, 4479.

[6] Z. Weng, Y. Su, D.-W. Wang, F. Li, J. Du, H.-M. Cheng, *Adv. Energy Mater.* **2011**, *1*, 917.

[7] S. Afroj, S. Tan, A. M. Abdelkader, K. S. Novoselov, N. Karim, *Adv. Funct. Mater.* **2020**, *30*, 2000293.

[8] P. Cataldi, P. Steiner, M. Liu, G. Pinter, A. Athanassiou, C. Kocabas, I. A. Kinloch, M. A. Bissett, *Adv. Funct. Mater.* **2023**, *33*, 2301542.

[9] P.-C. Hsu, X. Liu, C. Liu, X. Xie, H. R. Lee, A. J. Welch, T. Zhao, Y. Cui, *Nano Lett.* **2015**, *15*, 365.

[10] Y. Lian, H. Yu, M. Wang, X. Yang, Z. Li, F. Yang, Y. Wang, H. Tai, Y. Liao, J. Wu, X. Wang, Y. Jiang, G. Tao, *J. Mater. Chem. C* **2020**, *8*, 8399.

[11] M. Cao, M. Wang, L. Li, H. Qiu, M. A. Padhiar, Z. Yang, *Nano Energy* **2018**, *50*, 528.

[12] C. Wang, M. Zhang, K. Xia, X. Gong, H. Wang, Z. Yin, B. Guan, Y. Zhang, *ACS Appl. Mater. Interfaces* **2017**, *9*, 13331.

[13] D. V. Lam, S. Won, H. C. Shin, J.-H. Kim, S.-M. Lee, *Carbon* **2019**, *153*, 257.

[14] A. Sahasrabudhe, H. Dixit, R. Majee, S. Bhattacharyya, *Nat. Commun.* **2018**, *9*, 2014.

[15] Y. Zhu, M. Yang, Q. Huang, D. Wang, R. Yu, J. Wang, Z. Zheng, D. Wang, *Adv. Mater.* **2020**, *32*, 1906205.

[16] P. C. Ma, B. Z. Tang, J.-K. Kim, *Carbon* **2008**, *46*, 1497.

[17] X. Zhao, D. Madan, Y. Cheng, J. Zhou, H. Li, S. M. Thon, A. E. Bragg, M. E. DeCoster, P. E. Hopkins, H. E. Katz, *Adv. Mater.* **2017**, *29*, 1606928.

[18] H. Tang, Y. Liang, C. Liu, Z. Hu, Y. Deng, H. Guo, Z. Yu, A. Song, H. Zhao, D. Zhao, Y. Zhang, X. Guo, J. Pei, Y. Ma, Y. Cao, F. Huang, *Nature* **2022**, *611*, 271.

[19] Y. Kim, J. Zhu, B. Yeom, M. D. Prima, X. Su, J.-G. Kim, S. J. Yoo, C. Uher, N. A. Kotov, *Nature* **2013**, *500*, 59.

[20] Y. Ko, M. Kwon, W. K. Bae, B. Lee, S. W. Lee, J. Cho, *Nat. Commun.* **2017**, *8*, 536.

[21] S. Kang, D. Nam, J. Choi, J. Ko, D. Kim, C. H. Kwon, J. Huh, *ACS Appl. Mater. Interfaces* **2019**, *11*, 12032.

[22] Y. Song, D. Kim, S. Kang, Y. Ko, J. Ko, J. Huh, Y. Ko, S. W. Lee, J. Cho, *Adv. Funct. Mater.* **2019**, *29*, 1806584.

[23] S. Woo, D. Nam, W. Chang, Y. Ko, S. Lee, Y. Song, B. Yeom, J. H. Moon, S. W. Lee, J. Cho, *Small* **2021**, *17*, 2007579.

[24] Y. Ko, J. Park, J. Mo, S. Lee, Y. Song, Y. Ko, H. Lee, Y. Kim, J. Huh, S. W. Lee, J. Cho, *Adv. Funct. Mater.* **2021**, *31*, 2102530.

[25] D. Nam, M. Kwon, Y. Ko, J. Huh, S. W. Lee, J. Cho, *Appl. Phys. Rev.* **2021**, *8*, 011405.

[26] W. Chang, D. Nam, S. Lee, Y. Ko, C. H. Kwon, Y. Ko, J. Cho, *Adv. Sci.* **2022**, *9*, 2203800.

[27] S. Lee, Y. Ko, W. Chang, C. H. Kwon, Y. Kim, B. Yeom, J. Cho, *Chem. Eng. J.* **2023**, *454*, 140150.

[28] J. Ahn, Y. Song, Y. J. Kim, D. Nam, T. Kim, K. Kwak, C. H. Kwon, Y. Ko, S. J. Lee, J. Cho, *Chem. Eng. J.* **2023**, *455*, 140742.

[29] E. Yong, D. Nam, Y. Kim, K. Kim, B.-H. Kim, Y. Ko, J. Cho, *Energy Storage Mater.* **2023**, *60*, 102813.

[30] C. Hwang, W.-J. Song, J.-G. Han, S. Bae, G. Song, N.-S. Choi, S. Park, H.-K. Song, *Adv. Mater.* **2018**, *30*, 1705445.

[31] P. Gao, S. Xu, Z. Chen, X. Huang, Z. Bao, C. Lao, G. Wu, Y. Mei, *ACS Appl. Mater. Interfaces* **2018**, *10*, 3938.

[32] K. Jost, C. R. Perez, J. K. McDonough, V. Presser, M. Heon, G. Dion, Y. Gogotsi, *Energy Environ. Sci.* **2011**, *4*, 5060.

[33] K. Jost, G. Dion, Y. Gogotsi, *J. Mater. Chem. A* **2014**, *2*, 10776.

[34] K. Dong, X. Peng, Z. L. Wang, *Adv. Mater.* **2020**, *32*, 1902549.

[35] G. Chen, X. Xiao, X. Zhao, T. Tat, M. Bick, J. Chen, *Chem. Rev.* **2022**, *122*, 3259.

[36] B. Yao, J. Zhang, T. Kou, Y. Song, T. Liu, Y. Li, *Adv. Sci.* **2017**, *4*, 1700107.

[37] C. Wu, T. W. Kim, F. Li, T. Guo, *ACS Nano* **2016**, *10*, 6449.

[38] B. Dudem, A. R. Mule, H. R. Patnam, J. S. Yu, *Nano Energy* **2019**, *55*, 305.

[39] T. Lee, W. Lee, S.-W. Kim, J. J. Kim, B.-S. Kim, *Adv. Funct. Mater.* **2016**, *26*, 6206.

[40] J. D. Ryan, D. A. Mengistie, R. Gabrielsson, A. Lund, C. Müller, *ACS Appl. Mater. Interfaces* **2017**, *9*, 9045.

[41] E. Barjasteh, C. Sutanto, D. Nepal, *Langmuir* **2019**, *35*, 2261.

[42] S. Xu, Y. Yao, Y. Guo, X. Zeng, S. D. Lacey, H. Song, C. Chen, Y. Li, J. Dai, Y. Wang, Y. Chen, B. Liu, K. Fu, K. Amine, J. Lu, L. Hu, *Adv. Mater.* **2018**, *30*, 1704907.

**ADVANCED
SCIENCE NEWS**

www.advancedsciencenews.com

**small
structures**

www.small-structures.com

[43] L. Hu, J. W. Choi, Y. Yang, S. Jeong, F. La Mantia, L.-F. Cui, Y. Cui, *Proc. Natl. Acad. Sci. U. S. A.* **2009**, *106*, 21490.

[44] L. Hu, M. Pasta, F. L. Mantia, L. Cui, S. Jeong, H. D. Deshazer, J. W. Choi, S. M. Han, Y. Cui, *Nano Lett.* **2010**, *10*, 708.

[45] J. Lim, D. S. Choi, G. Y. Lee, H. J. Lee, S. P. Sasikala, K. E. Lee, S. H. Kang, S. O. Kim, *ACS Appl. Mater. Interfaces* **2017**, *9*, 41363.

[46] K.-H. Choi, J. Yoo, C. K. Lee, S.-Y. Lee, *Energy Environ. Sci.* **2016**, *9*, 2812.

[47] S. Xu, Y. Yao, Y. Guo, X. Zeng, S. D. Lacey, H. Song, C. Chen, Y. Li, J. Dai, Y. Wang, Y. Chen, B. Liu, K. Fu, J. Amine, J. Lu, L. Hu, *Adv. Mater.* **2017**, *30*, 1704907.

[48] Y. Qi, Y. Xia, P. Li, Z. Wang, X. Ming, B. Wang, K. Shen, G. Cai, K. Li, Y. Gao, Y. Liu, C. Gao, Z. Xu, *Adv. Fiber Mater.* **2023**, *5*, 896.

[49] N. N. Jason, W. Shen, W. Cheng, *ACS Appl. Mater. Interfaces* **2015**, *7*, 16760.

[50] G. Hu, J. Kang, L. W. T. Ng, X. Zhu, R. C. T. Howe, C. G. Jones, M. C. Hersam, T. Hasan, *Chem. Soc. Rev.* **2018**, *47*, 3265.

[51] J. H. Kim, S. Lee, M. Wajahat, H. Jeong, W. S. Chang, H. J. Jeong, J.-R. Yang, J. T. Kim, S. K. Seol, *ACS Nano* **2016**, *10*, 8879.

[52] H. Jin, N. Matsuhisa, S. Lee, M. Abbas, T. Yokota, T. Someya, *Adv. Mater.* **2017**, *29*, 1605848.

[53] D. McManus, S. Vranic, F. Withers, V. Sanshez-Romaguera, M. Macucci, H. Yang, R. Sorrentino, K. Parvez, S.-K. Son, G. Iannaccone, K. Kostarelos, G. Fiori, C. Casiraghi, *Nat. Nanotechnol.* **2017**, *12*, 343.

[54] M. S. Sadi, E. Kumpikaitė, *Cellulose* **2023**, *30*, 7981.

[55] Q. Yu, P. Weng, L. Han, X. Yin, Z. Chen, X. Hu, L. Wang, H. Wang, *Cellulose* **2019**, *26*, 7523.

[56] R. M. A. P. Lima, J. J. Alcaraz-Espinoza, F. A. G. da Silva Jr., H. P. de Oliveira, *ACS Appl. Mater. Interfaces* **2018**, *10*, 13783.

[57] W.-W. Liu, X.-B. Yan, J.-E. Lang, C. Peng, Q.-J. Xue, *J. Mater. Chem.* **2012**, *22*, 17245.

[58] I. A. Sahito, K. C. Sun, A. A. Arbab, M. B. Qadir, Y. S. Choi, S. H. Jeong, *J. Power Sources* **2016**, *319*, 90.

[59] B. Y. Ahn, E. B. Duoss, M. J. Motala, X. Guo, S.-I. Park, Y. Xiong, J. Yoon, R. G. Nuzzo, J. A. Rogers, J. A. Lewis, *Science* **2009**, *323*, 1590.

[60] E. C. Garnett, W. Cai, J. J. Cha, F. Mahmood, S. T. Connor, M. G. Christoforo, Y. Cui, M. D. McGehee, M. L. Brongersma, *Nat. Mater.* **2012**, *11*, 241.

[61] J. H. Park, G.-T. Hwang, S. Kim, J. Seo, H.-J. Park, K. Yu, T.-S. Kim, K. J. Lee, *Adv. Mater.* **2017**, *29*, 1603473.

[62] S. Gong, W. Schwalb, Y. Wang, Y. Chen, Y. Tang, J. Si, B. Shirinzadeh, W. Cheng, *Nat. Commun.* **2013**, *5*, 3132.

[63] W. Jeong, S. Lee, H. Choi, J. Bae, S.-H. Lee, Y. Ma, S. Yoo, J.-H. Ha, J.-I. Hong, S. Park, K. Woo, J.-H. Choi, S. Lee, *Mater. Today* **2022**, *61*, 30.

[64] M. L. Allen, M. Aronniemi, T. Mattila, A. Alastalo, K. Ojanperä, M. Suhonen, H. Seppä, *Nanotechnology* **2008**, *19*, 175201.

[65] S. Magdassi, M. Grouchko, O. Berezin, A. Kamyshny, *ACS Nano* **2010**, *4*, 1943.

[66] M. Grouchko, A. Kamyshny, C. F. Mihailescu, D. F. Anghel, S. Magdassi, *ACS Nano* **2011**, *5*, 3354.

[67] H.-J. Hwang, H. Devaraj, C. Yang, Z. Gao, C.-H. Chang, H. Lee, R. Malhotra, *Sci. Rep.* **2018**, *8*, 17159.

[68] C. Zhang, L. McKeon, M. P. Kremer, S.-H. Park, O. Ronan, A. Seral-Ascaso, S. Barwich, C. Ó Coileáin, N. McEvoy, H. C. Nerl, B. Anasori, J. N. Coleman, Y. Gogotsi, V. Nicolosi, *Nat. Commun.* **2019**, *10*, 1795.

[69] S. Uzun, M. Schelling, K. Hantanasirisakul, T. S. Mathis, R. Askeland, G. Dion, Y. Gogotsi, *Small* **2021**, *17*, 2006376.

[70] Y. Shao, L. Wei, X. Wu, C. Jiang, Y. Yao, B. Peng, H. Chen, J. Huangfu, Y. Ying, C. J. Zhang, J. Ping, *Nat. Commun.* **2022**, *13*, 3223.

[71] S. P. Sreenilayam, É. McCarthy, L. Mckeon, O. Ronan, R. McCann, K. Fleischer, B. Freeland, V. Nicolosi, D. Brabazon, *Chem. Eng. J.* **2022**, *449*, 137817.

[72] G. Hu, T. Albrow-Owen, X. Jin, A. Ali, Y. Hu, R. C. T. Howe, K. Shehzad, Z. Yang, X. Zhu, R. I. Woodward, T.-C. Wu, H. Jussila, J.-B. Wu, P. Peng, P.-H. Tan, Z. Sun, E. J. R. Kelleher, M. Zhang, Y. Xu, T. Hasan, *Nat. Commun.* **2017**, *8*, 278.

[73] D. V. Wagle, G. A. Baker, *Mater. Horiz.* **2015**, *2*, 157.

[74] Y. Lu, J. Y. Huang, C. Wang, S. Sung, J. Lou, *Nat. Nanotechnol.* **2010**, *5*, 218.

[75] M. Grouchko, R. Roitman, X. Zhu, I. Popov, A. Kamyshny, H. Su, S. Magdassi, *Nat. Commun.* **2014**, *5*, 2994.

[76] Ph. Buffat, J.-P. Borel, *Phys. Rev. A* **1976**, *13*, 2287.

[77] S. Wünscher, R. Abbel, J. Perelaer, U. S. Schubert, *J. Mater. Chem. C* **2014**, *2*, 10232.

[78] J. Sudagar, J. Lian, W. Sha, *J. Alloy. Compd.* **2013**, *571*, 183.

[79] J. B. You, S. Y. Kim, Y. J. Park, Y. G. Ko, S. G. Im, *Langmuir*, **2014**, *30*, 916.

[80] Y.-H. Zhu, S. Yuan, D. Bao, Y.-B. Yin, H.-X. Zhong, X.-B. Zhang, J.-M. Yan, Q. Jiang, *Adv. Mater.* **2017**, *29*, 1603719.

[81] D. Wang, J. Sun, Q. Xue, Q. Li, Y. Guo, Y. Zhao, Z. Chen, Z. Huang, Q. Yang, G. Liang, B. Dong, C. Zhi, *Energy Storage Mater.* **2021**, *36*, 272.

[82] X. Pu, L. Li, H. Song, C. Du, Z. Zhao, C. Jiang, G. Cao, W. Hu, Z. L. Wang, *Adv. Mater.* **2015**, *27*, 2472.

[83] Y.-H. Lee, J.-S. Kim, J. Noh, I. Lee, H. J. Kim, S. Choi, J. Seo, S. Jeon, T.-S. Kim, J.-Y. Lee, J. W. Choi, *Nano Lett.* **2013**, *13*, 5753.

[84] J. Chang, J. Shang, Y. Sun, L. K. Ono, D. Wang, Z. Ma, Q. Huang, D. Chen, G. Liu, Y. Cui, Y. Qi, Z. Zheng, *Nat. Commun.* **2018**, *9*, 4480.

[85] Y. Farraj, A. Kanner, S. Magdassi, *ACS Appl. Mater. Interfaces* **2023**, *15*, 21651.

[86] L. Liu, Y. Yu, C. Yan, K. Li, Z. Zheng, *Nat. Commun.* **2015**, *6*, 7260.

[87] Y. Yu, C. Yan, Z. Zheng, *Adv. Mater.* **2014**, *26*, 5508.

[88] X. Lin, M. Wu, L. Zhang, D. Wang, *ACS Appl. Electron. Mater.* **2019**, *1*, 397.

[89] H. M. Lee, S.-Y. Choi, A. Jung, S. H. Ko, *Angew. Chem.* **2013**, *125*, 7872.

[90] S. M. Dezfuli, M. Sabzi, *Ceram. Int.* **2019**, *45*, 21835.

[91] X. Lu, W. Shang, G. Chen, H. Wang, P. Tan, X. Deng, H. Song, Z. Xu, J. Huang, X. Zhou, *ACS Appl. Electron. Mater.* **2021**, *3*, 1477.

[92] Z. H. Guo, M. Liu, Z. Cong, W. Guo, P. Zhang, W. Hu, X. Pu, *Adv. Mater. Technol.* **2020**, *5*, 2000544.

[93] Z. Wang, S. Ji, F. Liu, H. Wang, X. Wang, Q. Wang, B. G. Pollet, R. Wang, *ACS Appl. Mater. Interfaces* **2019**, *11*, 29791.

[94] Z. Kang, Y. He, J. Sang, H. Hirahara, D. Chen, *Adv. Mater. Interfaces* **2021**, *8*, 2100651.

[95] N. Kanani, *Electroplating: Basic Principles, Processes and Practice*, Elsevier Advanced Technology, Oxford, England **2004**.

[96] S. Strassburg, S. Zainuddin, T. Scheibel, *Adv. Energy Mater.* **2021**, *11*, 2100519.

[97] J. Mo, Y. Ko, Y. S. Yun, J. Huh, J. Cho, *Energy Environ. Sci.* **2022**, *15*, 3815.

[98] D. Shin, Y. Song, D. Nam, J. H. Moon, S. W. Lee, J. Cho, *J. Mater. Chem. A* **2021**, *9*, 2334.

[99] M. B. Vázquez-Santos, E. Geissler, K. László, J.-N. Rouzaud, A. Martínez-Alonso, J. M. D. Tascón, *J. Phys. Chem. C* **2012**, *116*, 257.

[100] C. Wang, X. Li, E. Gao, M. Jian, K. Xia, Q. Wang, Z. Xu, T. Ren, Y. Zhang, *Adv. Mater.* **2016**, *28*, 6640.

[101] W. W. Yu, Y. A. Wang, X. Peng, *Chem. Mater.* **2003**, *15*, 4300.

[102] D. Monego, T. Kister, N. Kirkwood, P. Mulvaney, A. Widmer-Cooper, T. Kraus, *Langmuir* **2018**, *34*, 12982.

[103] J. J. Richardson, J. Cui, M. Björnmalm, J. A. Braunger, H. Ejima, F. Caruso, *Chem. Rev.* **2016**, *116*, 14828.

[104] G. Decher, *Science* **1997**, *277*, 1232.

[105] J. Park, J. Park, S. H. Kim, J. Cho, J. Bang, *J. Mater. Chem.* **2010**, *20*, 2085.

[106] S. Srivastava, N. A. Kotov, *Acc. Chem. Res.* **2008**, *41*, 1831.

[107] S. W. Lee, B.-S. Kim, S. Chen, Y. Shao-Horn, P. T. Hammond, *J. Am. Chem. Soc.* **2009**, *131*, 671.

[108] G. Yin, Y. Wang, W. Wang, Z. Qu, D. Yu, *Adv. Mater. Interfaces* **2021**, *8*, 2001893.

[109] B.-S. Kim, S. W. Park, P. T. Hammond, *ACS Nano* **2008**, *2*, 386.

[110] Y. Ko, H. Baek, Y. Kim, M. Yoon, J. Cho, *ACS Nano* **2013**, *7*, 143.

[111] M. Yoon, J. Choi, J. Cho, *Chem. Mater.* **2013**, *25*, 1735.

[112] M. Park, Y. Kim, Y. Ko, S. Cheong, S. W. Ryu, J. Cho, *J. Am. Chem. Soc.* **2014**, *136*, 17213.

[113] Y. Ko, D. Shin, B. Koo, S. W. Lee, W.-S. Yoon, J. Cho, *Nano Energy* **2015**, *12*, 612.

[114] S. Cheong, J.-K. Kim, J. Cho, *Nanoscale* **2016**, *8*, 18315.

[115] S. Ghosh, L. Manna, *Chem. Rev.* **2018**, *118*, 7804.

[116] G. D. M. R. Dabera, M. Walker, A. M. Sanchez, H. J. Pereira, R. Beanland, R. A. Hatton, *Nat. Commun.* **2017**, *8*, 1894.

[117] N. C. Anderson, M. P. Hendricks, J. J. Choi, J. S. Owen, *J. Am. Chem. Soc.* **2013**, *135*, 18536.

[118] T. Hwang, J. S. Oh, J.-P. Hong, G.-Y. Nam, A.-H. Bae, S.-I. Son, G.-H. Lee, H.-K. Sung, Y. Lee, J.-D. Nam, *Carbon* **2012**, *50*, 612.

[119] K. S. Dijith, R. Aiswarya, C. V. Sruthi, S. Pillai, K. P. Surendran, *J. Ind. Eng. Chem.* **2020**, *88*, 196.

[120] K. Chen, R. Pathak, A. Gurung, K. M. Reza, N. Ghimire, J. Pokharel, A. Baniya, W. He, J. J. Wu, Q. Qiao, Y. Zhou, *J. Mater. Chem. A* **2020**, *8*, 1911.

[121] W. C. Li, C. L. Mak, C. W. Kan, C. Y. Hui, *RSC Adv.* **2014**, *4*, 64890.

[122] N. Ogihara, Y. Itou, T. Sasaki, Y. Takeuchi, *J. Phys. Chem. C* **2015**, *119*, 4612.

[123] H. Zheng, J. Li, X. Song, G. Liu, V. S. Battaglia, *Electrochim. Acta* **2012**, *71*, 258.

[124] F. Shen, W. Luo, J. Dai, Y. Yao, M. Zhu, E. Hitz, Y. Tang, Y. Chen, V. L. Sprenkle, X. Li, L. Hu, *Adv. Energy Mater.* **2016**, *6*, 1600377.

[125] S.-G. Woo, S. Yoo, S.-H. Lim, J.-S. Yu, K. Kim, J. Lee, D. Lee, J.-H. Kim, S.-Y. Lee, *Adv. Funct. Mater.* **2020**, *30*, 1908633.

[126] H.-W. Park, M.-S. Jang, J.-S. Choi, J. Pyo, C.-G. Kim, *Compos. Struct.* **2021**, *256*, 112999.

[127] D. P. Dubal, N. R. Chodankar, D.-H. Kim, P. Gomez-Romero, *Chem. Soc. Rev.* **2018**, *47*, 2065.

[128] K. Qi, R. Hou, S. Zaman, Y. Qiu, B. Y. Xia, H. Duan, *ACS Appl. Mater. Interfaces* **2018**, *10*, 18021.

[129] T. Qin, S. Peng, J. Hao, Y. Wen, Z. Wang, X. Wang, D. He, J. Zhang, J. Hou, G. Cao, *Adv. Energy Mater.* **2017**, *7*, 1700409.

[130] A. Laforgue, *J. Power Sources* **2011**, *196*, 559.

[131] Z.-H. Huang, Y. Song, X.-X. Xu, X.-X. Liu, *ACS Appl. Mater. Interfaces* **2015**, *7*, 25506.

[132] C. Wang, T. He, J. Cheng, Q. Guan, B. Wang, *Adv. Funct. Mater.* **2020**, *30*, 2004430.

[133] S. Wang, J. Shen, Q. Wang, Y. Fan, L. Li, K. Zhang, L. Yang, W. Zhang, X. Wang, *ACS Appl. Energy Mater.* **2019**, *2*, 1077.

[134] X. Zhu, Y. Zhang, Z. Man, W. Lu, W. Chen, J. Xu, N. Bao, W. Chen, G. Wu, *Adv. Mater.* **2023**, 2307186.

[135] M. Barakzehi, M. Montazer, F. Sharif, T. Norby, A. Chatzitakis, *Electrochim. Acta* **2020**, *336*, 135743.

[136] M. D. Musick, C. D. Keating, L. A. Lyon, S. L. Botsko, D. J. Peña, W. D. Holliway, T. M. McEvoy, J. N. Richardson, M. J. Natan, *Chem. Mater.* **2000**, *12*, 2869.

[137] J. W. Ostrander, A. A. Mamedov, N. A. Kotov, *J. Am. Chem. Soc.* **2001**, *123*, 1101.

[138] J. D. Bernal, J. Mason, *Nature* **1960**, *188*, 910.

[139] M. Kwon, D. Nam, S. Lee, Y. Kim, B. Yeom, J. H. Moon, S. W. Lee, Y. Ko, J. Cho, *Adv. Energy Mater.* **2021**, *11*, 2101631.

[140] Y. Yue, H. Liang, *Small Methods* **2018**, *2*, 1800056.

[141] L.-F. Chen, Z.-Y. Yu, X. Ma, Z.-Y. Li, S.-H. Yu, *Nano Energy* **2014**, *9*, 345.

[142] L. Shen, B. Ding, P. Nie, G. Cao, X. Zhang, *Adv. Energy Mater.* **2013**, *3*, 1484.

[143] N. Yu, H. Yin, W. Zhang, Y. Liu, Z. Tang, M.-Q. Zhu, *Adv. Energy Mater.* **2016**, *6*, 1501458.

[144] Y. Song, T. Liu, B. Yao, M. Li, T. Kou, Z.-H. Huang, D.-Y. Feng, F. Wang, Y. Tong, X.-X. Liu, Y. Li, *ACS Energy Lett.* **2017**, *2*, 1752.

[145] Y. Gogotsi, P. Simon, *Science* **2011**, *334*, 917.

[146] M. D. Stoller, R. S. Ruoff, *Energy Environ. Sci.* **2010**, *3*, 1294.

[147] G. Wang, L. Zhang, J. Zhang, *Chem. Soc. Rev.* **2012**, *41*, 797.

[148] T. Brezesinski, J. Wang, S. H. Tolbert, B. Duun, *Nat. Mater.* **2010**, *9*, 146.

[149] A. E. Fischer, M. P. Saunders, K. A. Pettigrew, D. R. Rolison, J. W. Long, *J. Elctrochem. Soc.* **2008**, *155*, A246.

[150] P. Poizot, S. Laruelle, S. Grugeon, L. Dupont, J.-M. Tarascon, *Nature* **2000**, *407*, 496.

[151] R. Malik, D. Burch, M. Bazant, G. Ceder, *Nano Lett.* **2010**, *10*, 4123.

[152] G. He, L. F. Nazar, *ACS Energy Lett.* **2017**, *2*, 1122.

[153] Y. Song, S. Lee, Y. Ko, J. Huh, Y. Kim, B. Yeom, J. H. Moon, J. Cho, *Adv. Funct. Mater.* **2022**, *32*, 2106438.

[154] U. Simon, *Adv. Mater.* **1998**, *10*, 1487.

[155] P. R. Bueno, J. J. Davis, *Chem. Soc. Rev.* **2020**, *49*, 7505.

[156] T. Yamamoto, T. Maruyama, Z.-H. Zhou, T. Ito, T. Fukuda, Y. Yoneda, F. Begum, T. Ikeda, S. Sasaki, H. Takezoe, A. Fukuda, K. Kubota, *J. Am. Chem. Soc.* **1994**, *116*, 4832.

[157] S. Sivaramakrishnan, P.-J. Chia, Y.-C. Yeo, L.-L. Chua, P. K.-H. Ho, *Nat. Mater.* **2007**, *6*, 149.

[158] F. Dubois, B. Mahler, B. Dubertret, E. Doris, C. Mioskowski, *J. Am. Chem. Soc.* **2007**, *129*, 482.

[159] Y. Ko, M. Kwon, Y. Song, S. W. Lee, J. Cho, *Adv. Funct. Mater.* **2018**, *28*, 1804926.

[160] S. Sun, *Adv. Mater.* **2006**, *18*, 393.

[161] M. Wühn, J. Weckesser, C. Wöll, *Langmuir* **2001**, *17*, 7605.

[162] K. De Nolf, S. M. Cosseddu, J. J. Jasieniak, E. Drijvers, J. C. Martins, I. Infante, Z. Hens, *J. Am. Chem. Soc.* **2017**, *139*, 3456.

[163] P. Gao, Z. Chen, Z. Zhao-Karger, J. E. Mueller, C. Jung, S. Klyatskaya, T. Diemant, O. Fuhr, T. Jacob, R. J. Behm, M. Ruben, M. Fichtner, *Angew. Chem.* **2017**, *129*, 10477.

[164] J. Yun, Y. Song, I. Cho, Y. Ko, C. H. Kwon, J. Cho, *Nanoscale* **2019**, *11*, 17815.

[165] J. Choi, D. Nam, D. Shin, Y. Song, C. H. Kwon, I. Cho, S. W. Lee, J. Cho, *ACS Nano* **2019**, *13*, 12719.

[166] Y. Song, W. Bae, J. Ahn, Y. Son, M. Kwon, C. H. Kwon, Y. Kim, Y. Ko, J. Cho, *Adv. Sci.* **2023**, *10*, 202301248.

[167] B. L.-H. Hu, F.-Y. Wu, C.-T. Lin, A. N. Khlobystov, L.-J. Li, *Nat. Commun.* **2013**, *4*, 1687.

[168] S. W. Lee, B. M. Gallant, Y. Lee, N. Yoshida, D. Y. Kim, Y. Yamada, S. Noda, A. Yamada, Y. Shao-Horn, *Energy Environ. Sci.* **2012**, *5*, 5437.

[169] X. Li, L. Yuan, R. Liu, H. He, J. Hao, Y. Lu, Y. Wang, G. Liang, G. Yuan, Z. Guo, *Adv. Energy Mater.* **2021**, *11*, 2003010

[170] J. Lv, P. Zhou, L. Zhang, Y. Zhong, X. Sui, B. Wang, Z. Chen, H. Xu, Z. Mao, *Chem. Eng. J.* **2019**, *361*, 897.

[171] Z.-H. Huang, Y. Song, D.-Y. Feng, Z. Sun, X. Sun, X.-X. Liu, *ACS Nano* **2018**, *12*, 3557.

[172] G. Nagaraju, S. C. Sekhar, L. K. Bharat, J. S. Yu, *ACS Nano* **2017**, *11*, 10860.

[173] L. Wang, X. Feng, L. Ren, Q. Piao, J. Zhong, Y. Wang, H. Li, Y. Chen, B. Wang, *J. Am. Chem. Soc.* **2015**, *137*, 4920.

[174] X. Zheng, W. Nie, Q. Hu, X. Wang, Z. Wang, L. Zou, X. Hong, H. Yang, J. Shen, C. Li, *Mater. Des.* **2021**, *200*, 109442.

[175] M.-X. Guo, S.-W. Bian, F. Shao, S. Liu, Y.-H. Peng, *Electrochim. Acta* **2016**, *209*, 486.

[176] M. S. Javed, J. Chen, L. Chen, Y. Xi, C. Zhang, B. Wang, C. Hu, *J. Mater. Chem. A* **2016**, *4*, 667.

[177] J. Zhu, S. Tang, J. Wu, X. Shi, B. Zhu, X. Meng, *Adv. Energy Mater.* **2017**, *7*, 1601234.

[178] O. Okhay, A. Tkach, M. J. H. Gallo, G. Otero-Irurueta, S. Mikhalev, P. Staiti, F. Lufrano, *J. Energy Storage* **2020**, *32*, 101839.

[179] Z. Liu, K. Huang, J. Kang, L. Liu, S. Wang, C. Xiong, *Appl. Surf. Sci.* **2021**, *567*, 150761.

[180] L. Hu, F. L. Mantia, H. Wu, X. Xie, J. McDonough, M. Pasta, Y. Cui, *Adv. Energy Mater.* **2011**, *1*, 1012.

[181] Q. Cheng, Z. Song, T. Ma, B. B. Smith, R. Tang, H. Yu, H. Jiang, C. K. Chan, *Nano Lett.* **2013**, *13*, 4969.

[182] X. Shan, S. Zhang, N. Zhang, Y. Chen, H. Gao, X. Zhang, *J. Colloid Interface Sci.* **2018**, *510*, 327.

[183] D. Zhao, J. Qin, L. Zheng, D. Guo, J. Wang, M. Cao, *Nano Res.* **2021**, *14*, 4336.

[184] Y. Wu, S. S. Mechael, Y. Chen, T. B. Carmichael, *ACS Appl. Mater. Interfaces* **2020**, *12*, 51679.

[185] T. Gao, C. Xu, R. Li, R. Zhang, B. Wang, X. Jiang, M. Hu, Y. Bando, D. Kong, P. Dai, X.-B. Wang, *ACS Nano* **2019**, *13*, 11901.

[186] B. Zhao, X. Deng, R. Ran, M. Liu, Z. Shao, *Adv. Energy Mater.* **2015**, *6*, 1500924.

Woojae Chang is a Ph.D. candidate under the supervision of Prof. Jinhan Cho at the Department of Chemical and Biological Engineering in Korea University. Currently, his research is focused on the development of novel textile energy electrodes and their energy storage applications using a ligand replacement reaction-based layer-by-layer assembly.

Euiju Yong is a Ph.D. candidate under the supervision of Prof. Jinhan Cho at the Department of Chemical and Biological Engineering in Korea University. Currently, her research interest is focused on textile-based lithium ion battery electrodes based on the interfacial engineering of functional nanomaterials.

Yoon Jang Chung is an assistant professor at the Department of Chemical & Biological Engineering in Korea University. He received his B.S. and M.S. degrees from Seoul National University in 2010 and 2012. Then, he worked at the Korea Research Institute for Chemical Technology until 2015 before moving to Princeton University to receive his Ph.D. in 2021. Prior to joining Korea University, he was a post-doctoral scholar at the Laboratory for Physical Sciences in Maryland. His research focuses on the deposition and characterization of functional thin films, with an emphasis on their electronic properties.

Yongmin Ko received his Ph.D. degree at the Department of Chemical and Biological Engineering in Korea University in 2016. He was a postdoctoral researcher at Georgia Institute of Technology in Atlanta until 2019. Currently, he is working as a senior researcher at the Division of Energy Technology at the Daegu Gyeongbuk Institute of Science and Technology (DGIST) in Republic of Korea. His research interest is focused on energy conversion and storage devices based on various functional nanomaterials.

2300330 (24 of 25)
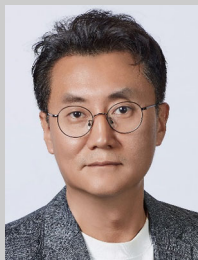
Jinhan Cho is a professor at the Department of Chemical & Biological Engineering in Korea University since 2010. His research career started in POSTECH and Seoul National University, where he completed M.S. and Ph.D. degrees in 1997 and 2001, respectively. Then, he had post-doc courses at Max-Planck-Institute of Colloids and Interface and University of Melbourne. In 2003–2005, he was a senior researcher in LG Chemistry R&D center. In 2006–2010, he had worked as an assistant professor in Kookmin University. His research interests have been focused on surface chemistry and electrochemical properties of various electrode materials.

2300330 (25 of 25)